

Diamond X-Ray Diagnostics Building a Better Beam

Using the tools of materials science to improve user facilities from electron sources to beam diagnostics

John Smedley

Brookhaven National Laboratory

Technologies for NSLS-II and LCLS-II

Maybe useful for MaRIE?

- Diamond based x-ray beam diagnostics
 - Theory
 - Flux, position & timing
 - X-ray absorption Spectroscopy
 - Beam imaging!
- Electron Sources
 - Needs for high brightness & role of roughness
 - Source of roughness in alkali antimonides
 - Possible solutions

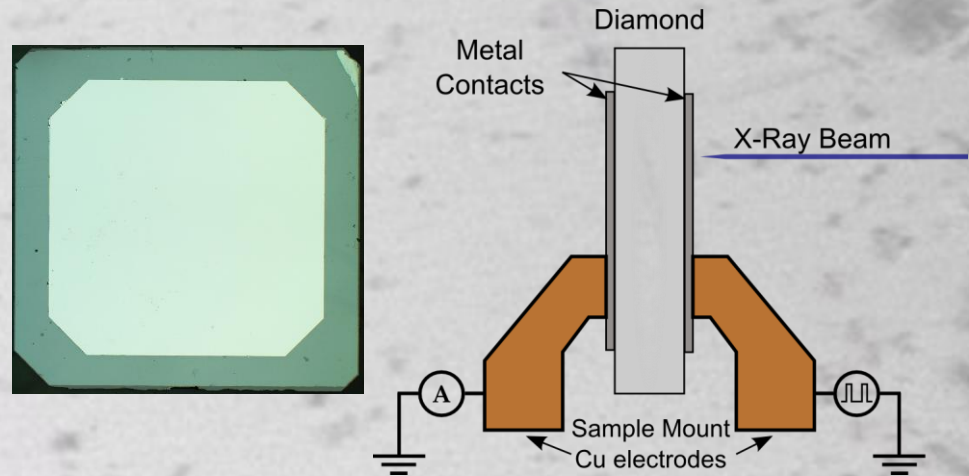
Diamond as a X-ray sensor

Diamond Advantages:

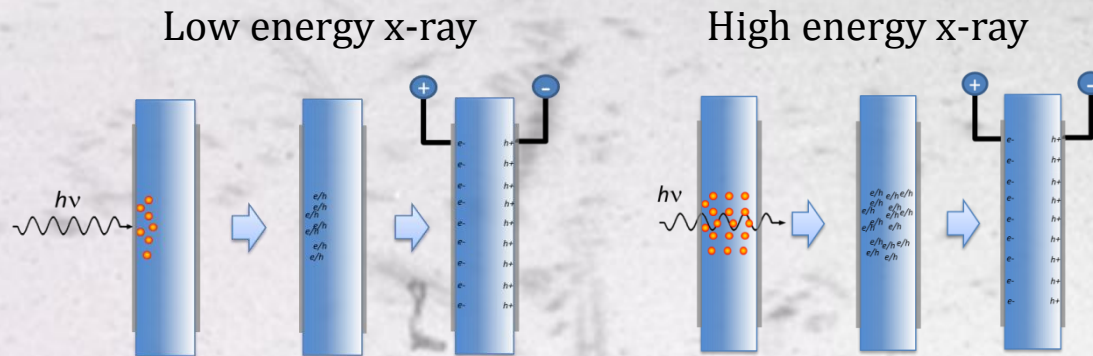
- Low X-ray Absorption
- High Thermal Conductivity
- Mechanical Strength
- Radiation Hardness
- Indirect bandgap

Sample Information:

- Electrical grade CVD single crystal diamond
- (100) surface orientation
- ~1 ppb nitrogen impurity
- Typical size: 4mm x 4mm x 50 μ m



X-ray generated charge carriers



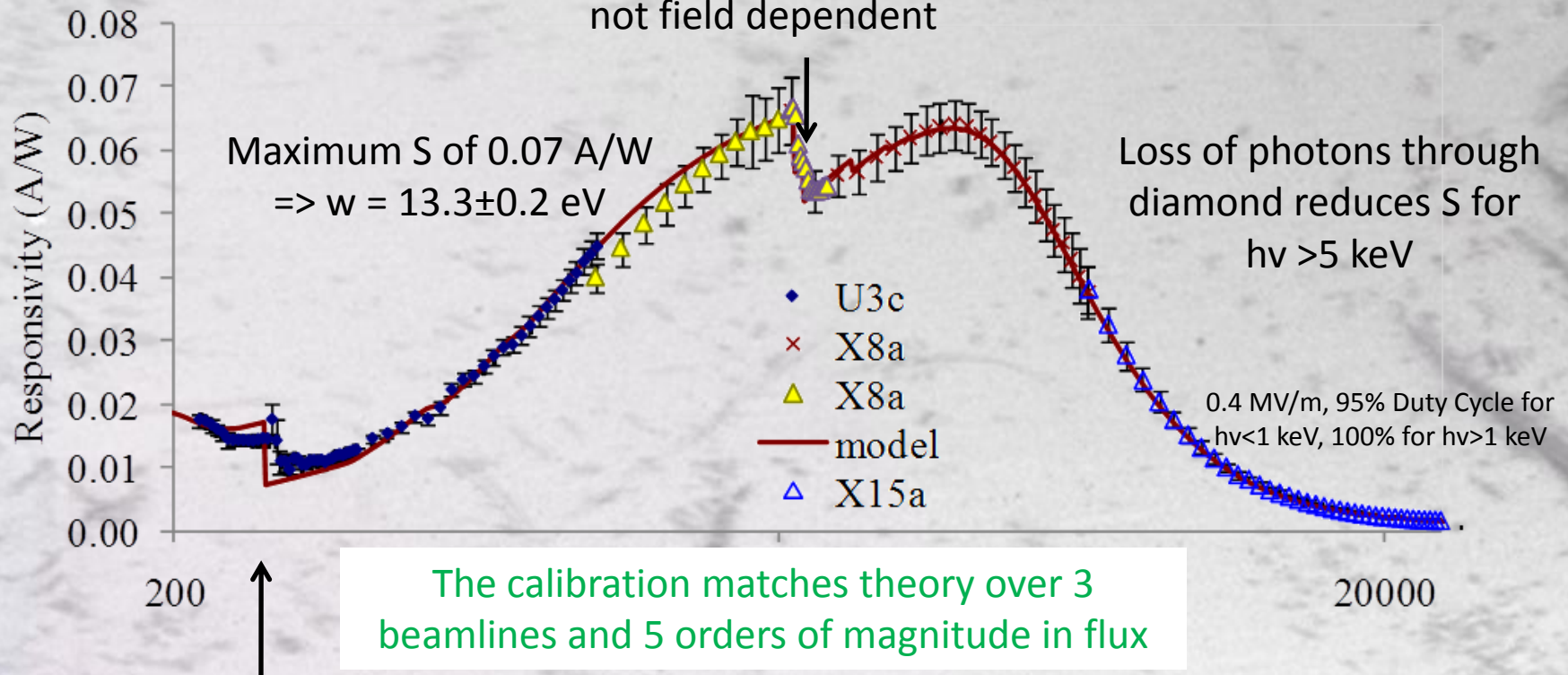
Electron hole pairs created near incident electrode: must move entire thickness of the diamond

Electron hole pairs created throughout the thickness creating a column of electron-hole pairs

Responsivity vs Photon Energy

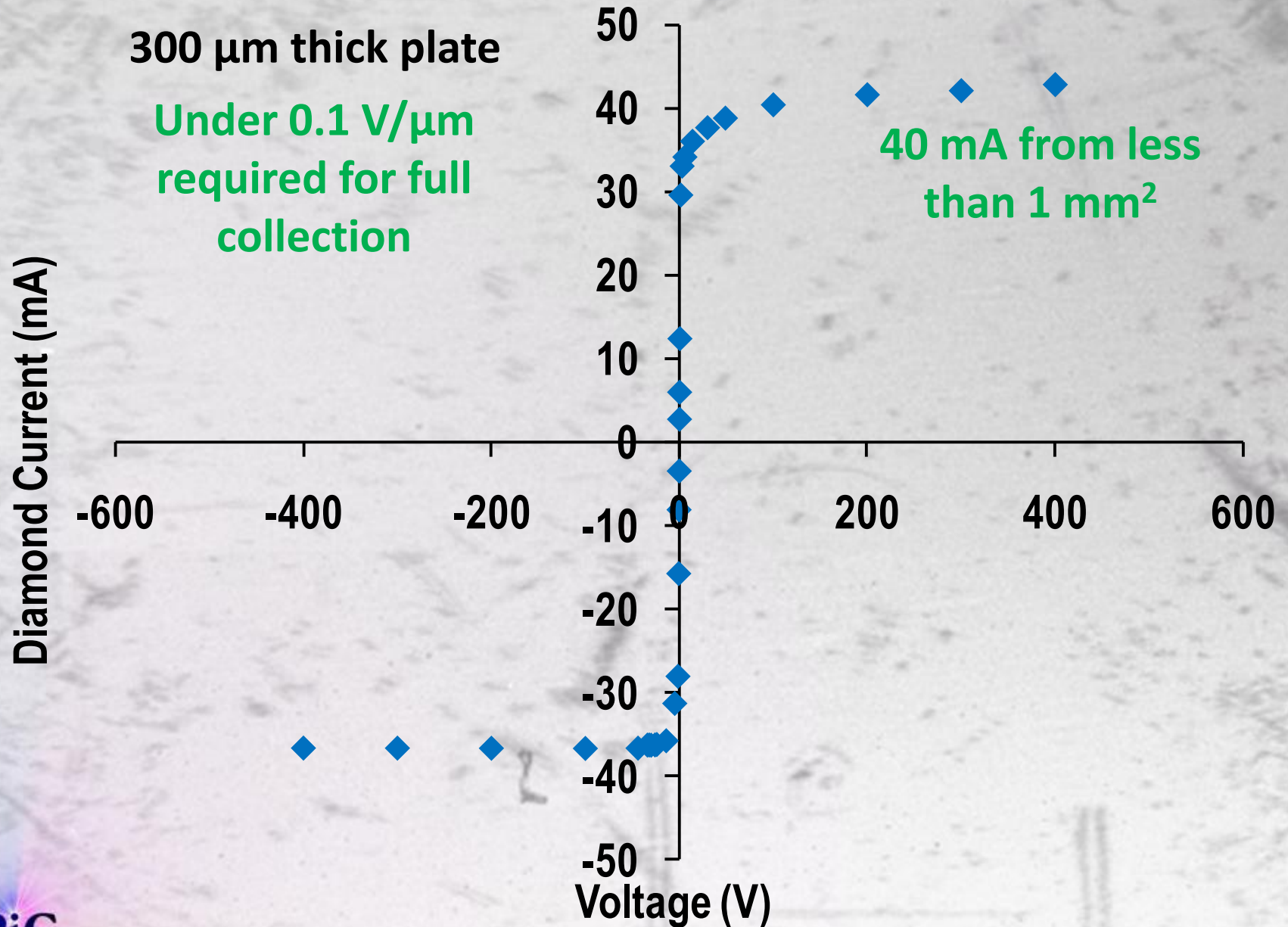
$$S = \frac{1}{w} e^{-t_{\text{metal}}/\lambda_{\text{metal}}} \left(1 - e^{-t_{\text{dia}}/\lambda_{\text{dia}}}\right) CE[\nu, F]$$

Platinum M edge feature due to loss of photons absorbed by incident contact
not field dependent

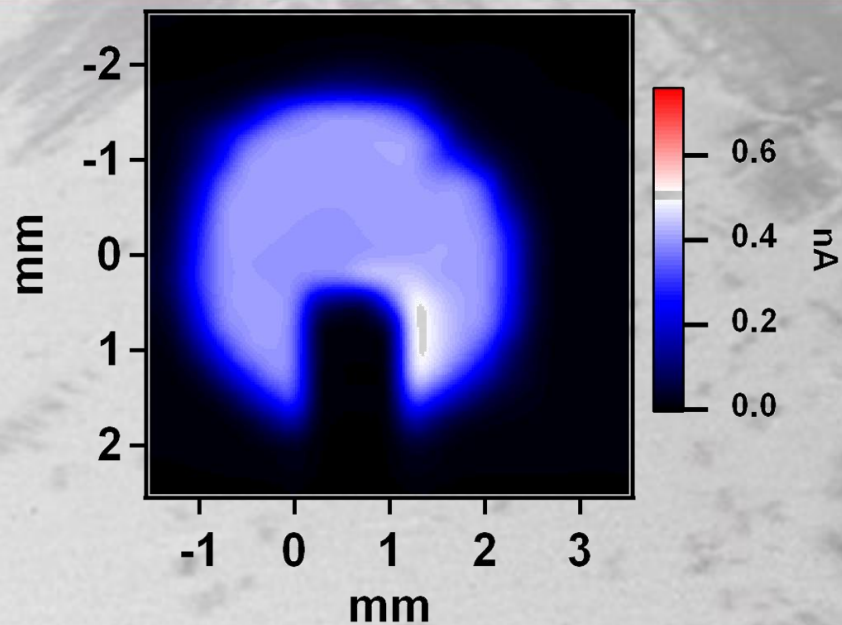
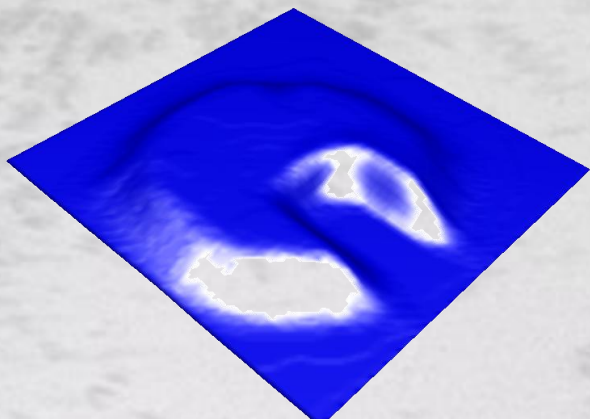


C K edge feature is field dependent, caused by incomplete carrier collection for carriers produced near incident electrode – electrons diffuse into incident contact and are lost

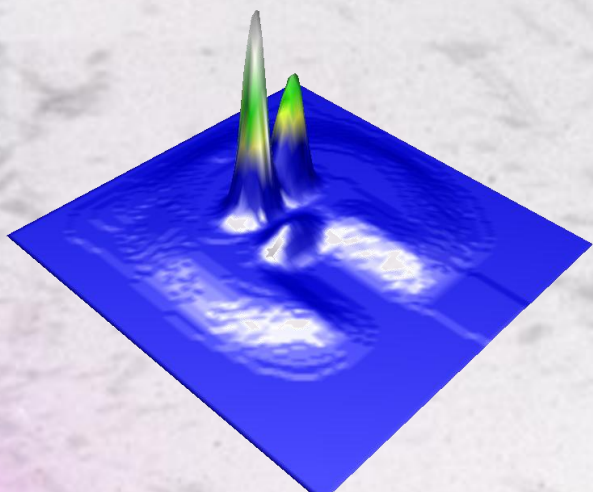
Response vs Bias



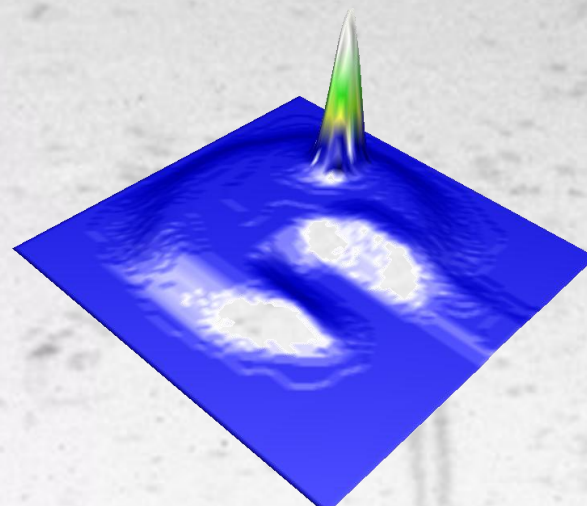
HID14 in X15
(80%, 100V, 1kHz, 19keV)



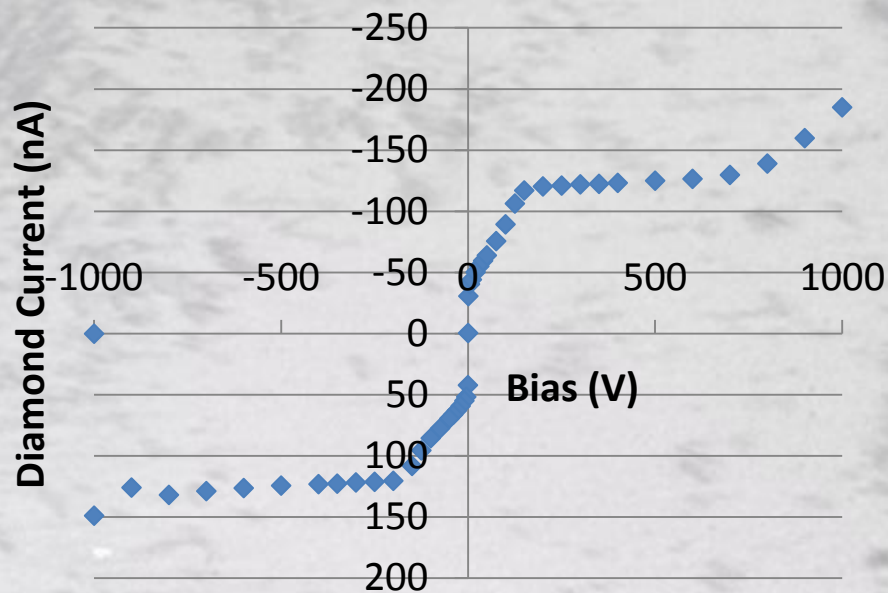
HID18 in X6B
(80% , -100V, 1kHz, 19keV)



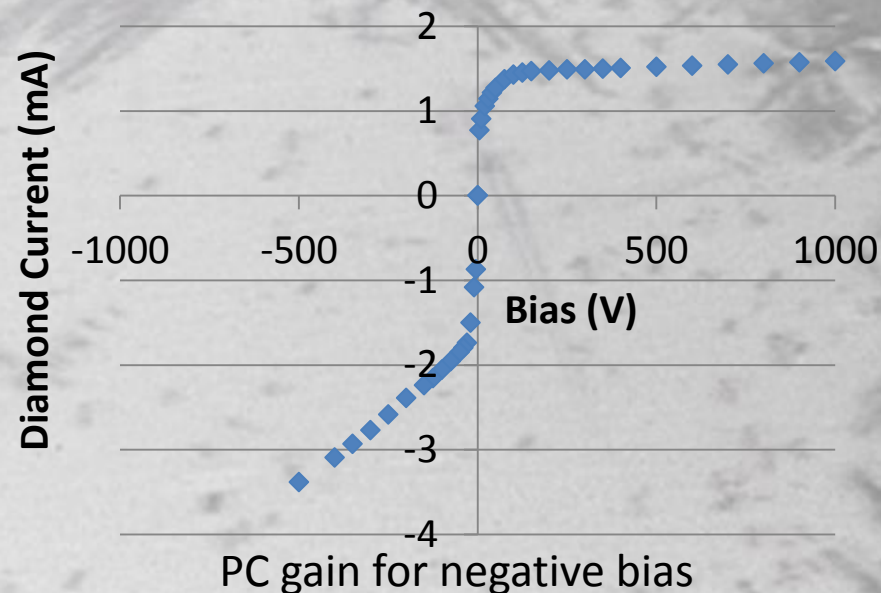
HID18 in X6B
(80% , +100V, 1kHz, 19keV)



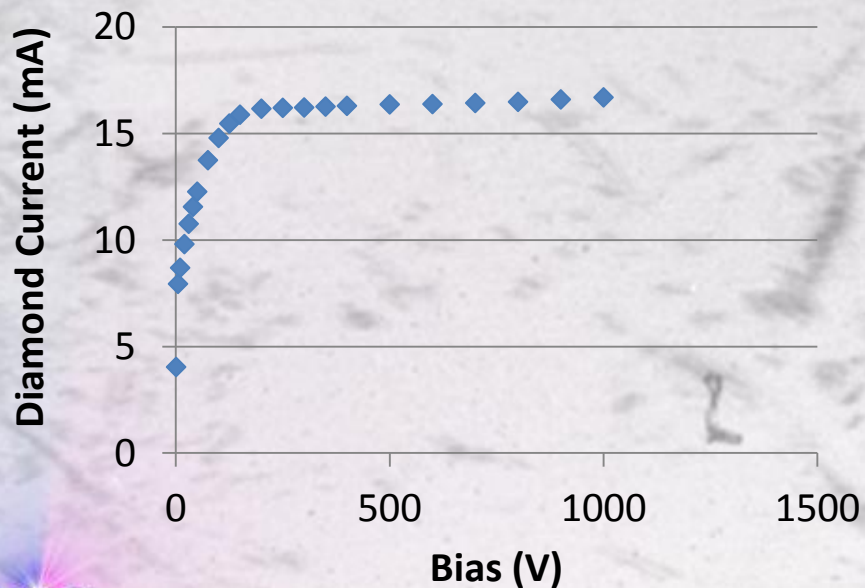
4.5 mm Al attenuator



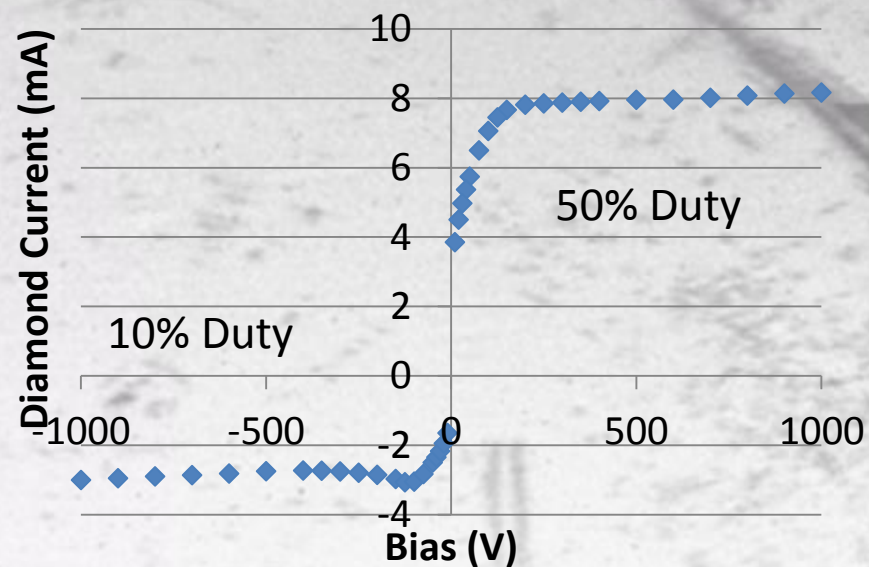
0.25 mm Al attenuator



No Filter

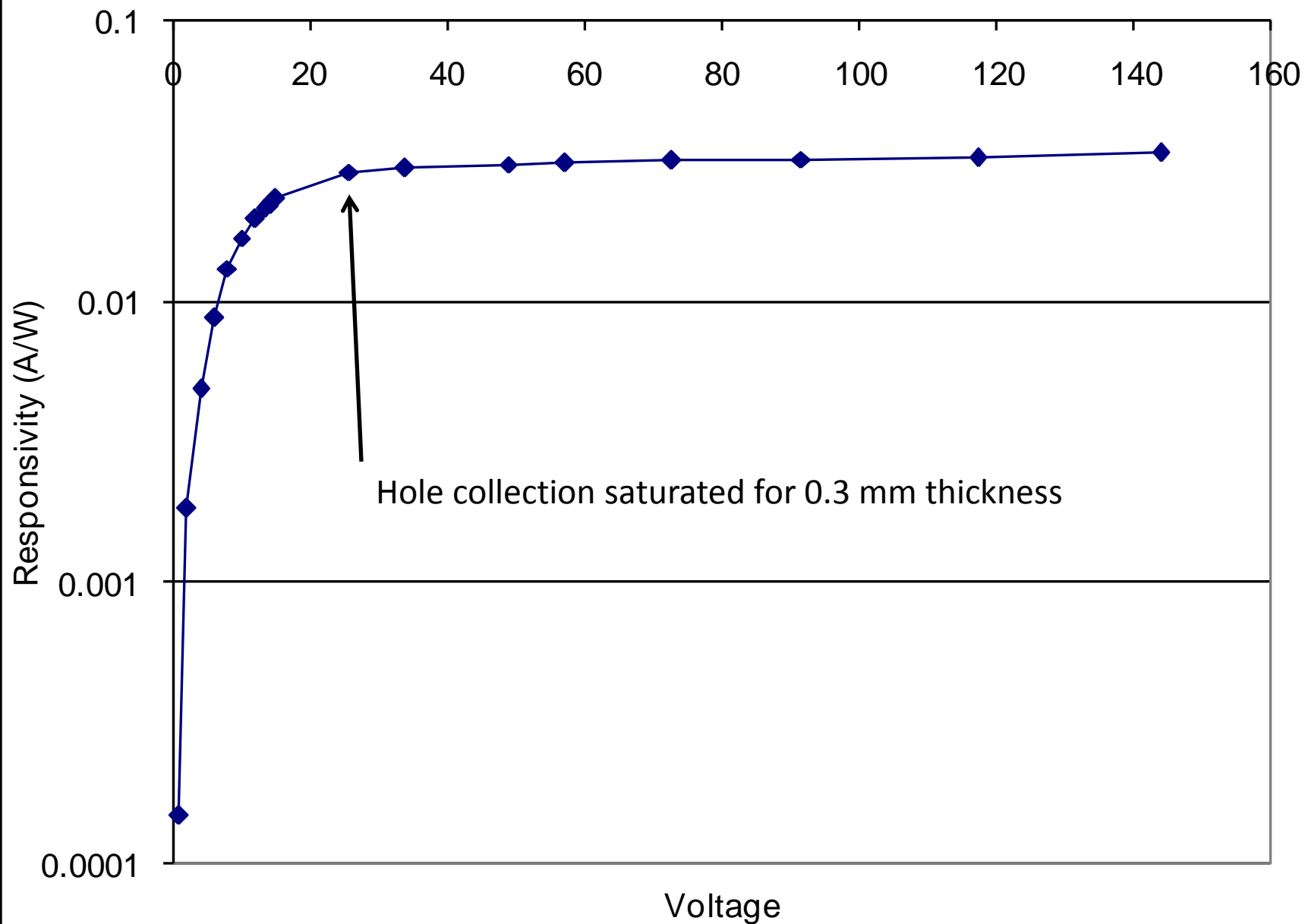


Full Beam



PC gain removed by operating at low Duty Cycle

Hole Response (1 keV)



What about electrons?

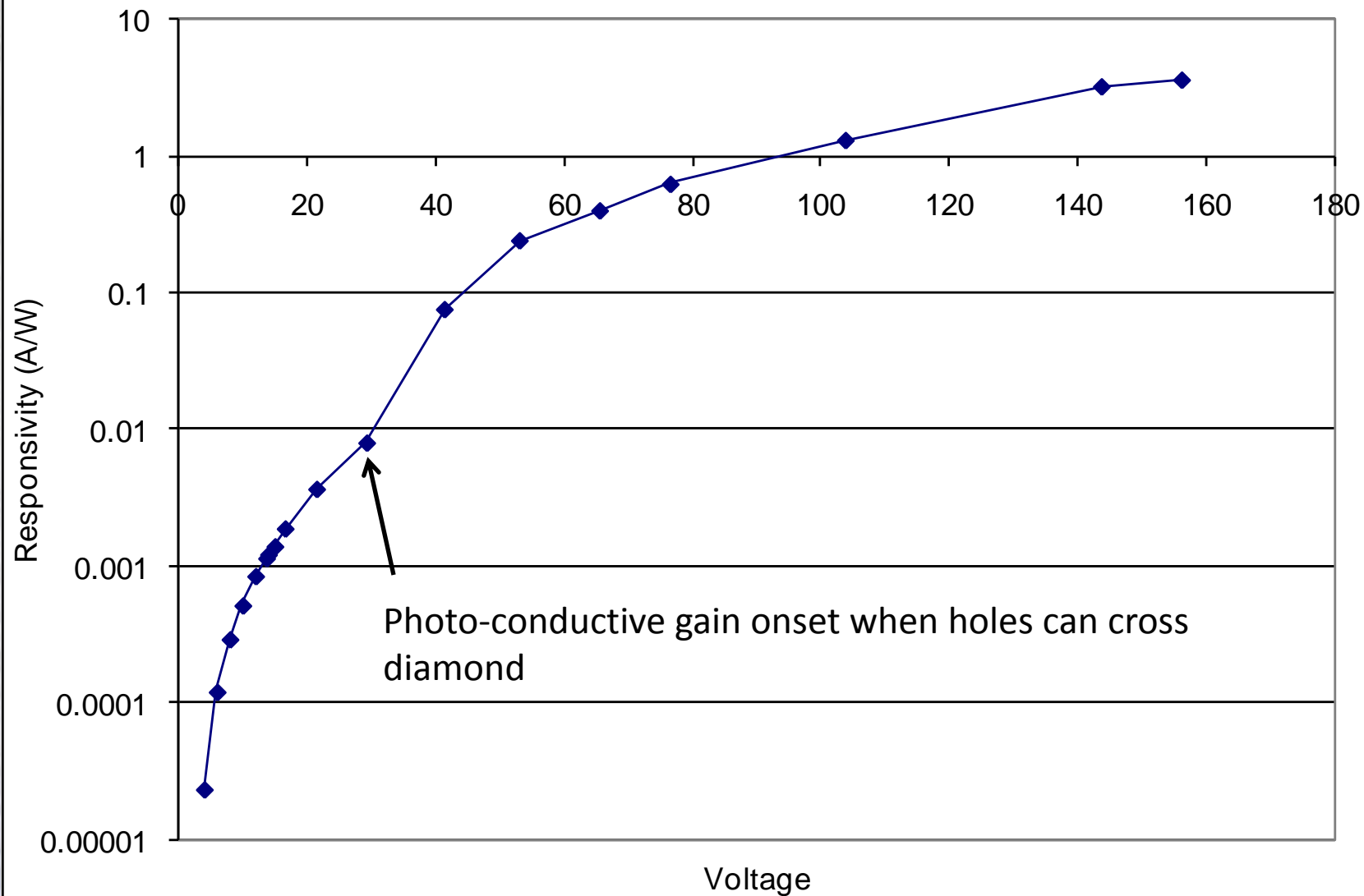
- Electron response depends strongly on type of electrical contacts
- For blocking contacts (Pt on O-terminated diamond), electrons exhibit significantly more trapping than holes
 - Lower duty cycle of pulsed bias to avoid signal loss
- For injecting contacts, photoconductive gain is observed
 - Trapped electrons act as effective “doping” of material
 - Holes are injected from opposite electrode

$$Gain = \frac{\tau_{holes}}{t_{holes}}$$

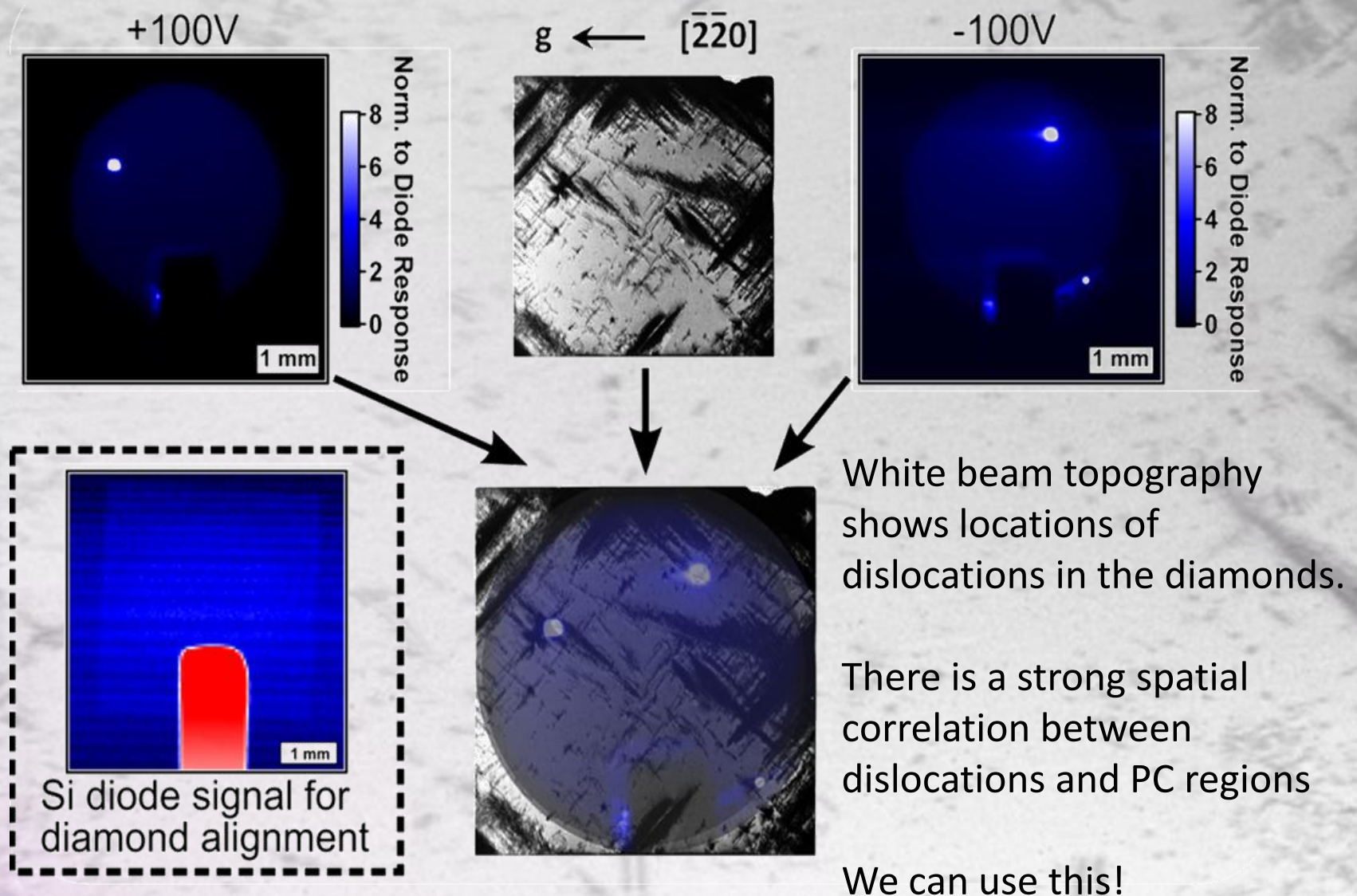
Hole lifetime

Hole transit time

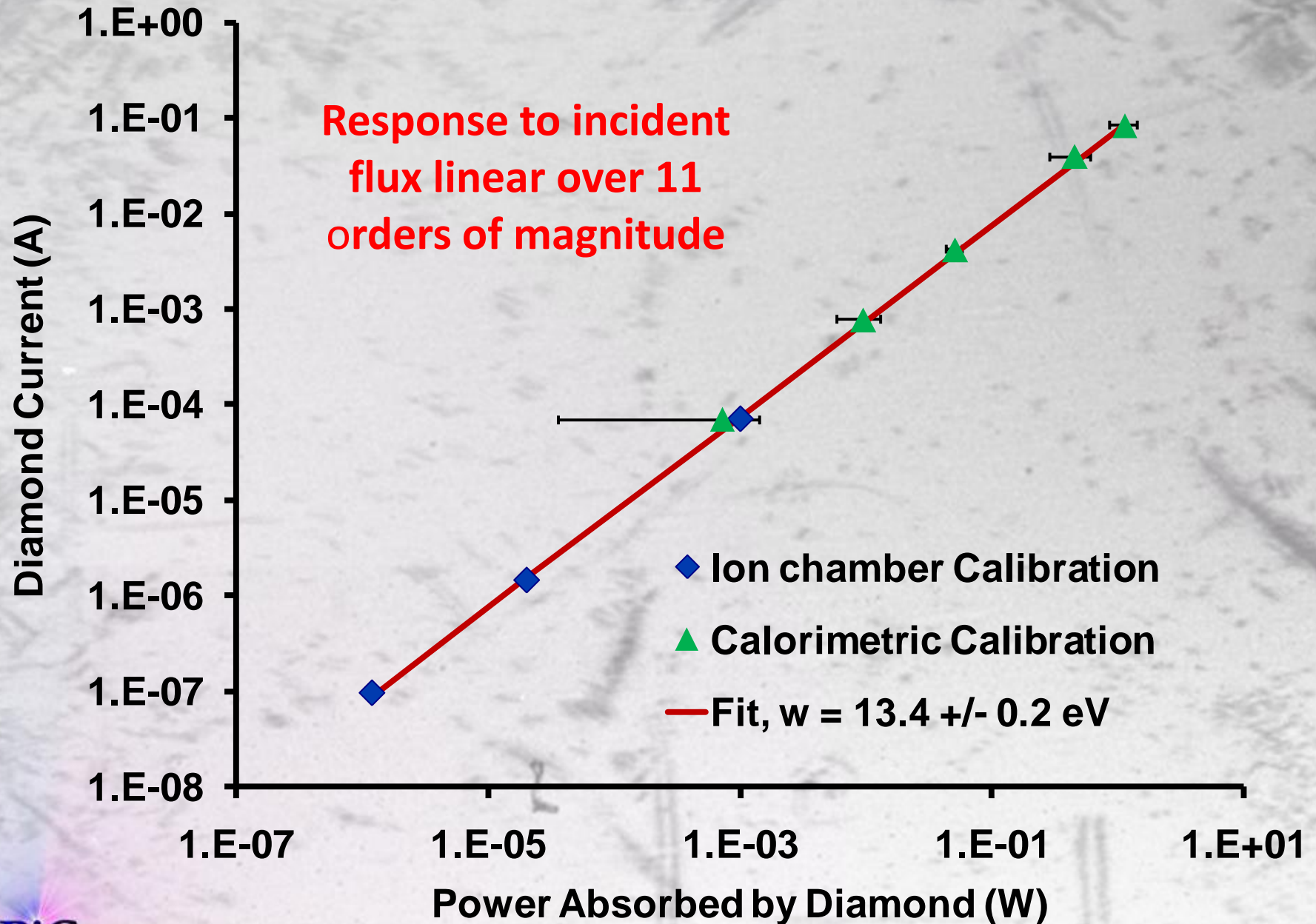
Electron Response (1 keV)



Relation to Threading Dislocations

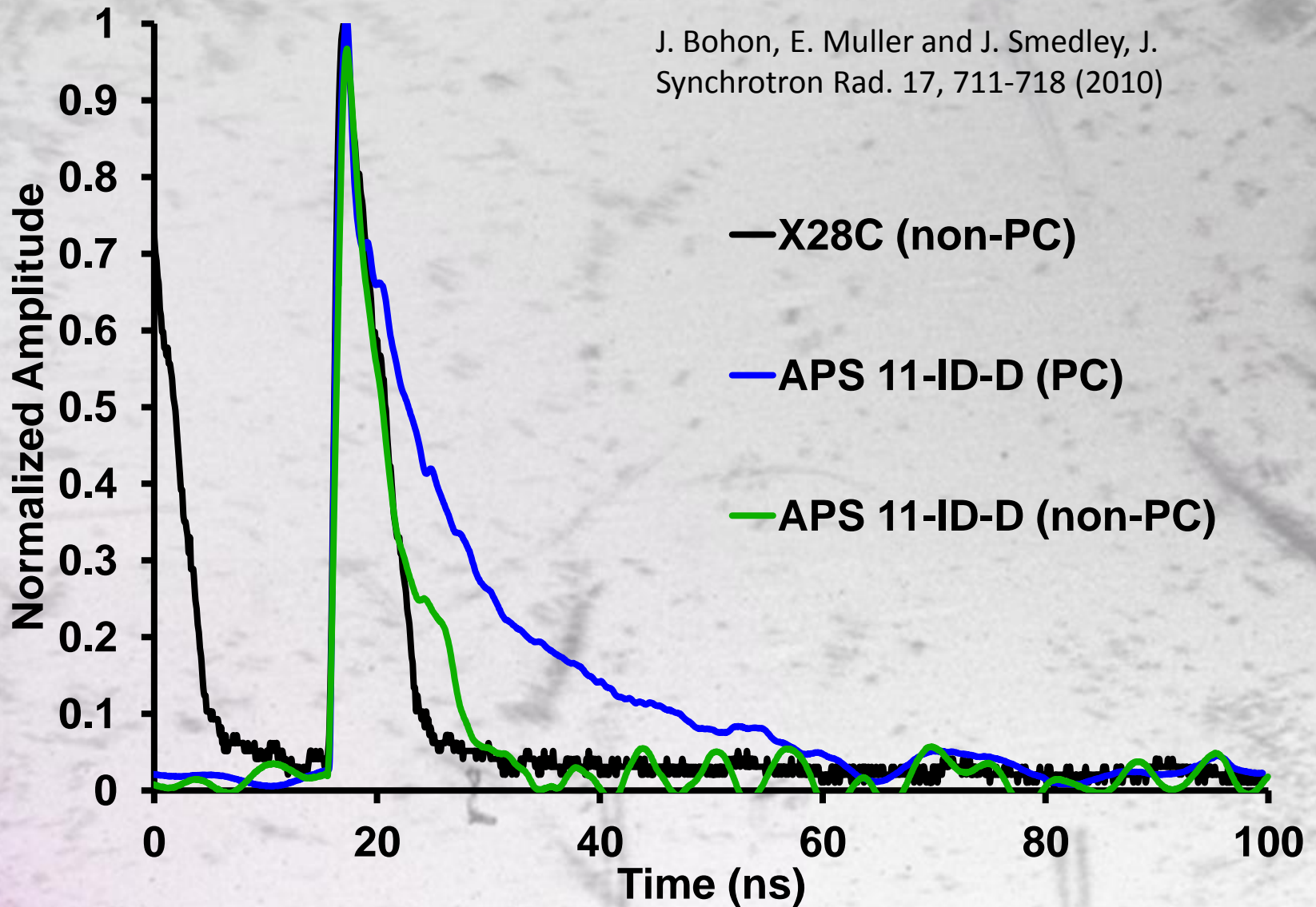


High Flux Response

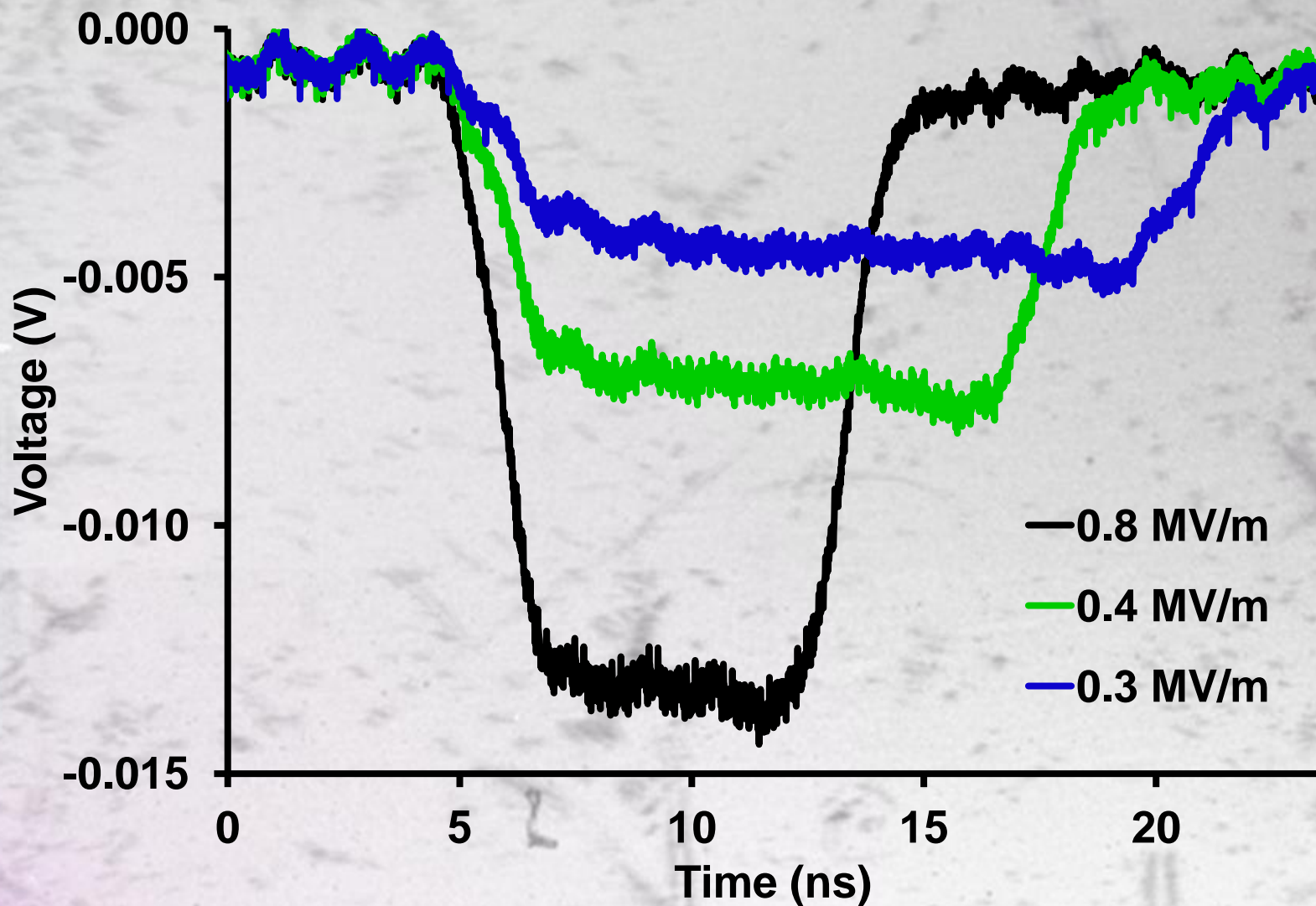


Temporal Response, Hard X-rays

J. Bohon, E. Muller and J. Smedley, J.
Synchrotron Rad. 17, 711-718 (2010)



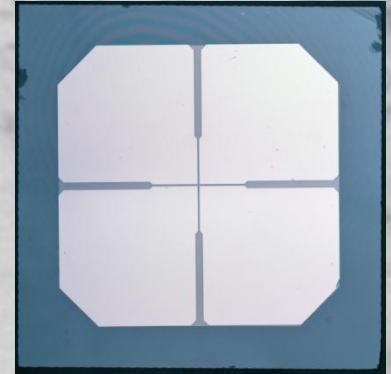
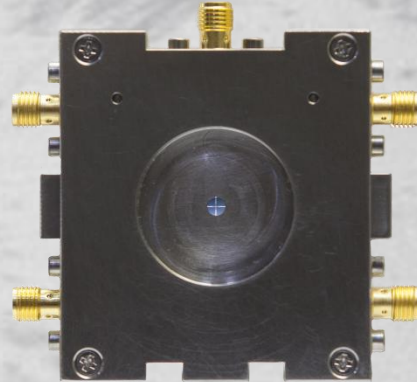
Temporal Response, Soft X-rays



Diamond Beam Position Monitors

❖ Circuit Board Mounted

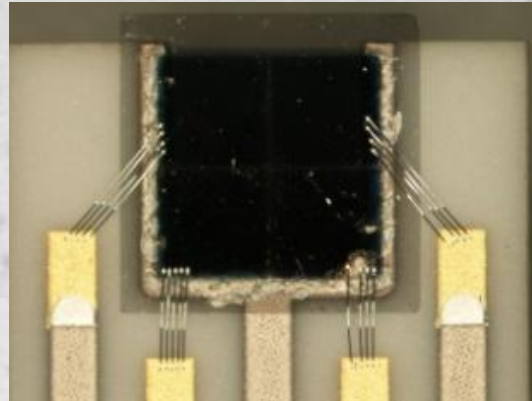
- ❖ Pt metallization
- ❖ wire-bonded electrodes
- ❖ SMA/LEMO connectors



❖ Application specific –

X-Ray fluorescence (X27)

- ❖ Ag diamond metallization
- ❖ Ceramic board
- ❖ 1 cm wide (compact)
- ❖ Ag traces



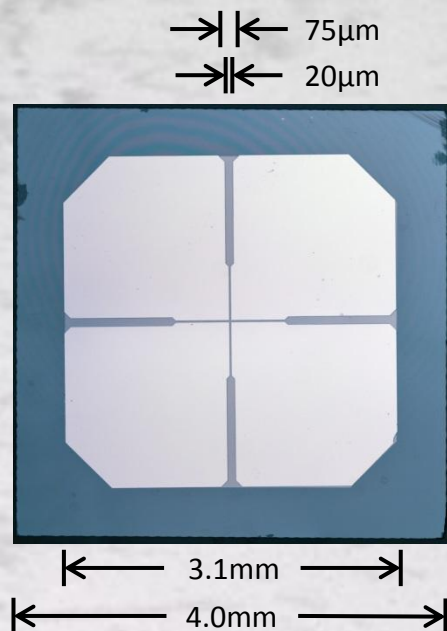
❖ White BPM (X25)

- ❖ Mini-gap undulator
- ❖ ~100W incident power
- ❖ Large beam



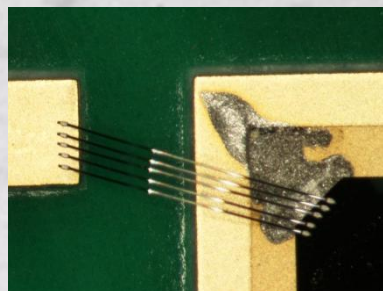
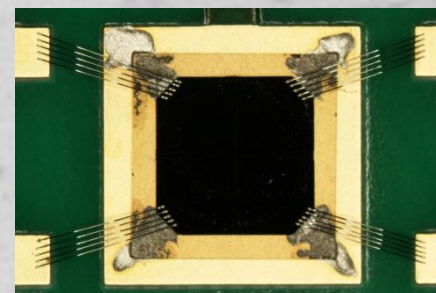
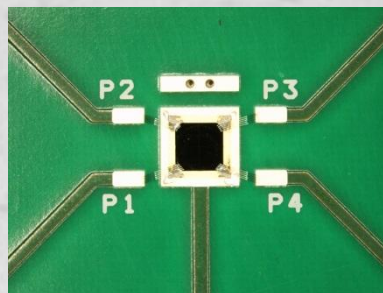
Fabrication

Lithography @ CFN



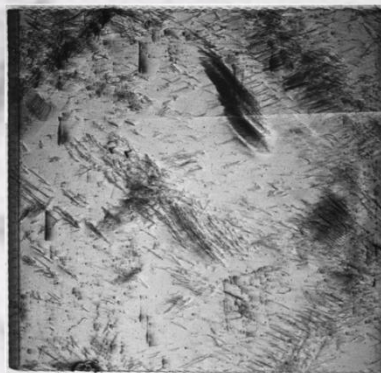
Electronic grade single crystal
(100) diamond
30-50 μm thick
20 μm street over a 1mm
center region
Metalization: 25 nm Pt

Wire Bonding - Instrumentation



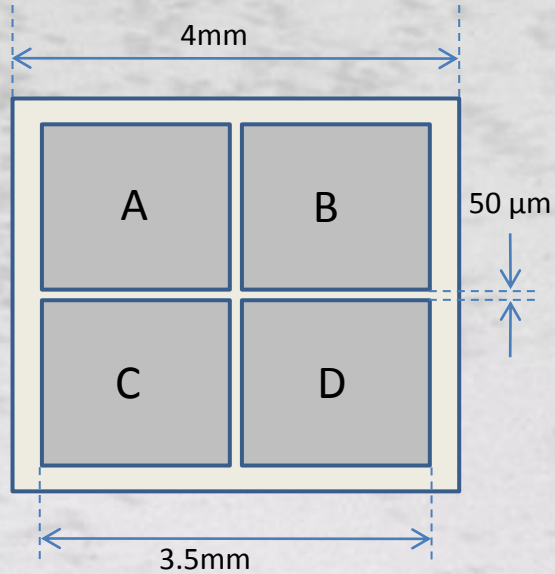
25 μm aluminum
wirebonds
5 bonds per pad
Conductive epoxy for
backside/bias contacts

Topography – NSLS/CHESS

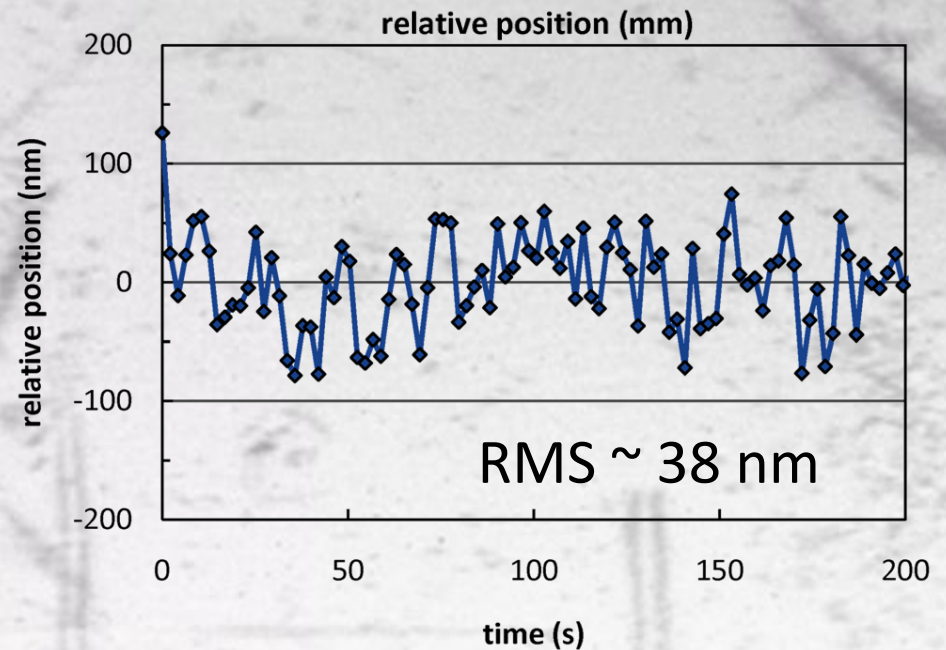
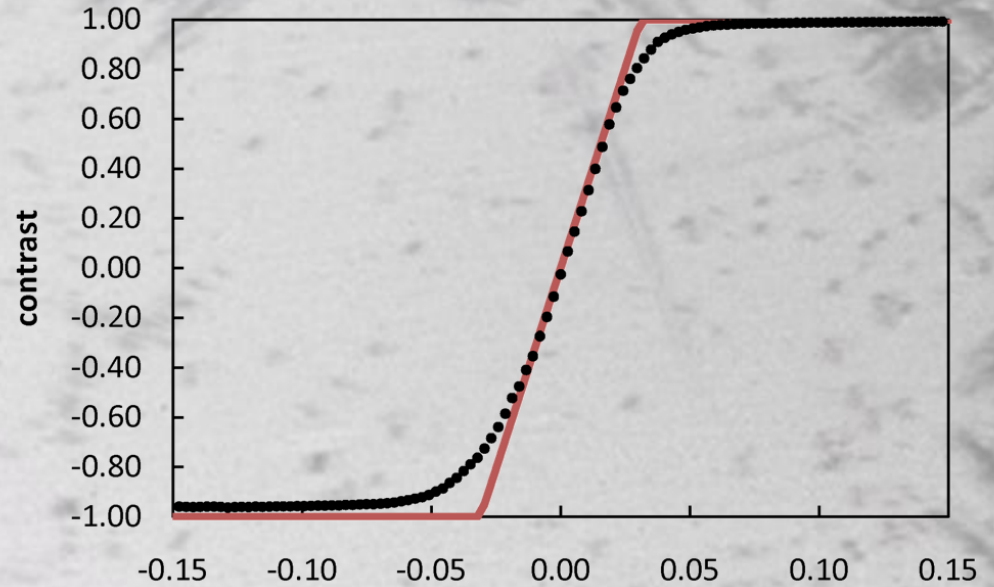
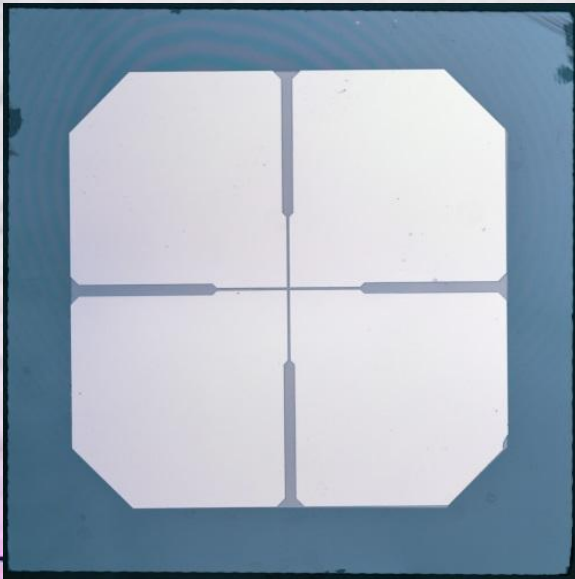


White beam topography
Prior to slicing

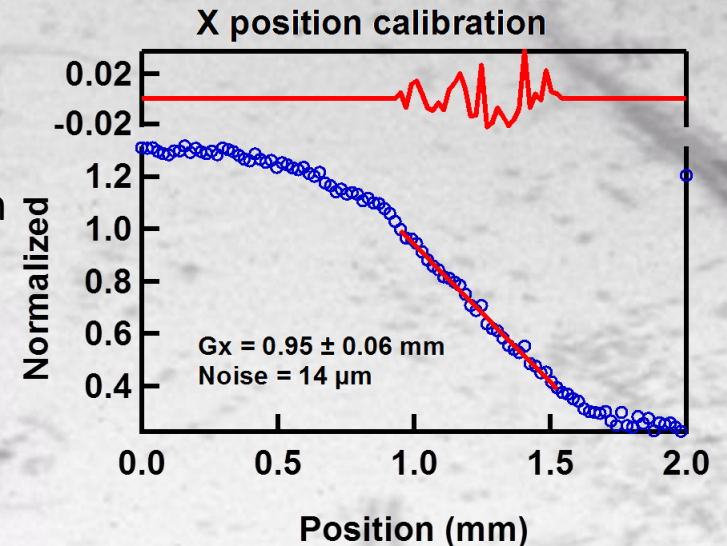
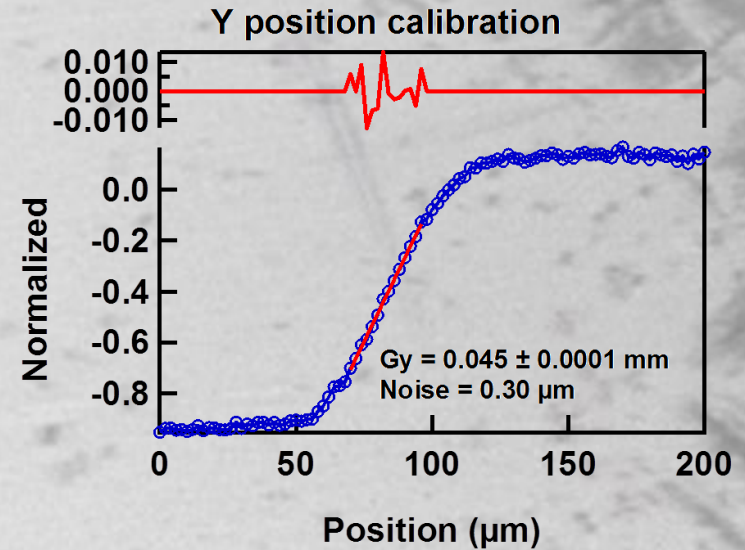
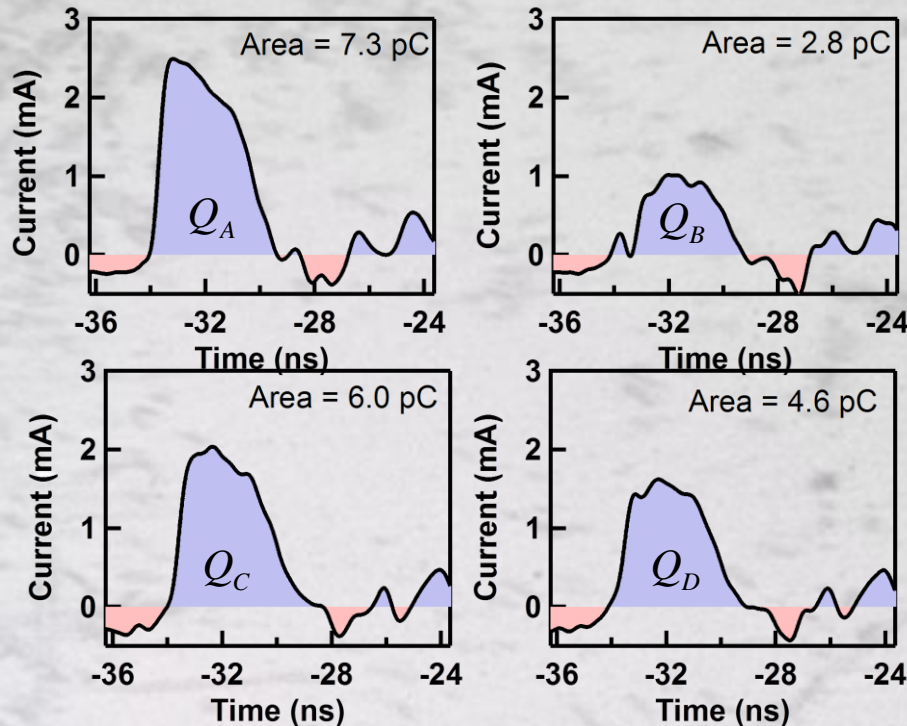
Beam Position Monitors



$$X = G_x \frac{(I_B + I_D) - (I_A + I_C)}{I_A + I_B + I_C + I_D}$$



Pulse Mode Beam Position



- Area under pulse (charge) was used to calculate position
- G_x and G_y were calculated by using:

$$X = G_x \frac{(Q_B + Q_D) - (Q_A + Q_C)}{Q_A + Q_B + Q_C + Q_D} \quad Y = G_y \frac{(Q_A + Q_B) - (Q_C + Q_D)}{Q_A + Q_B + Q_C + Q_D}$$

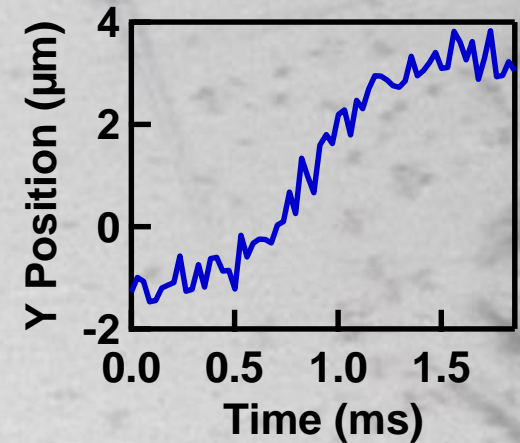
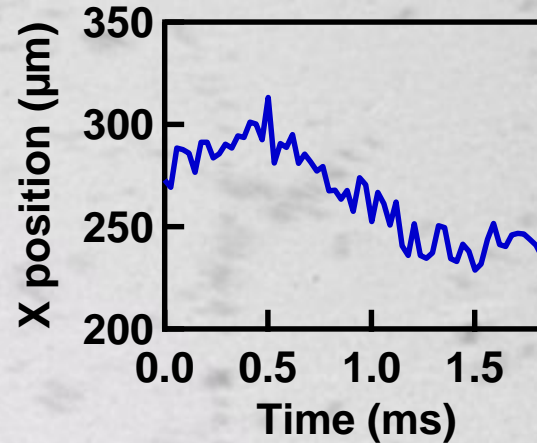
- Position noise was calculated by taking the standard deviation of the residuals and multiplying by G
 - Includes all noise sources, including actual beam wander

Position Stability at 11-ID-D, APS

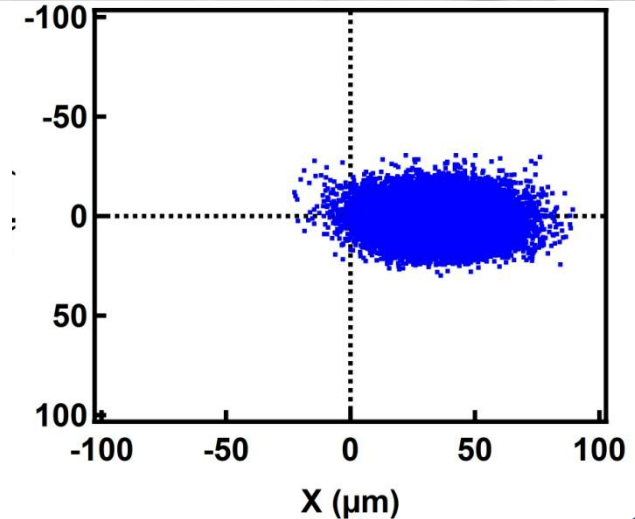
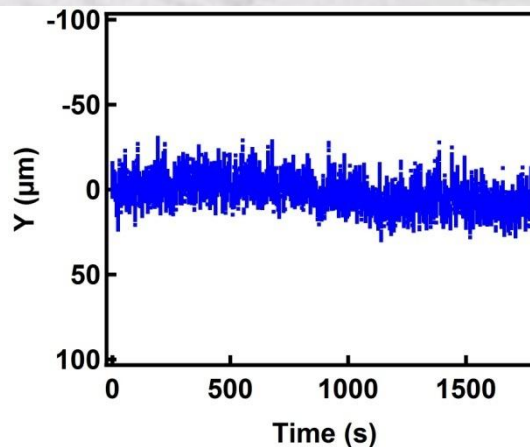
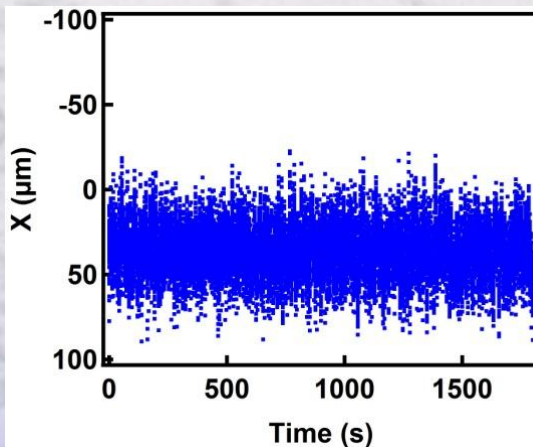
Ring Structure at APS 11-ID-D

- 24 bunches spaced 153 ns apart
- Takes 3.68 μs to complete one orbit
- Beam size 15 μm x 0.8 mm
- Measured the position of the first bunch continuously
- +400V on quad (~ 2 MV/m)
- Recently acquired 324 mode

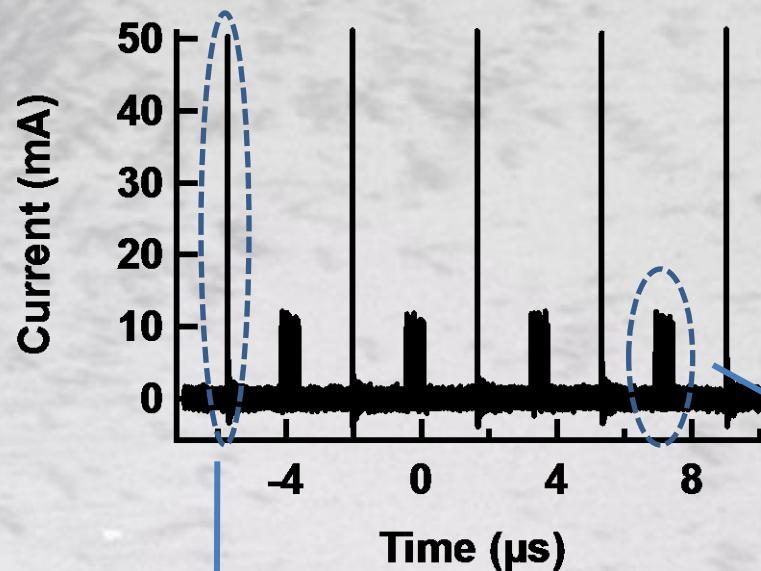
Short term stability



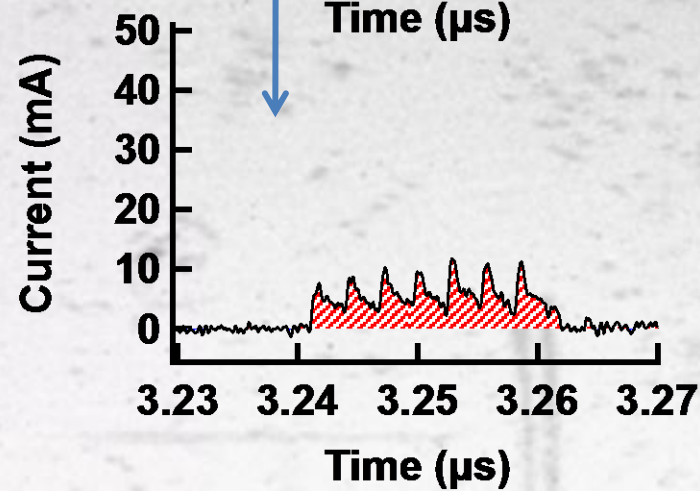
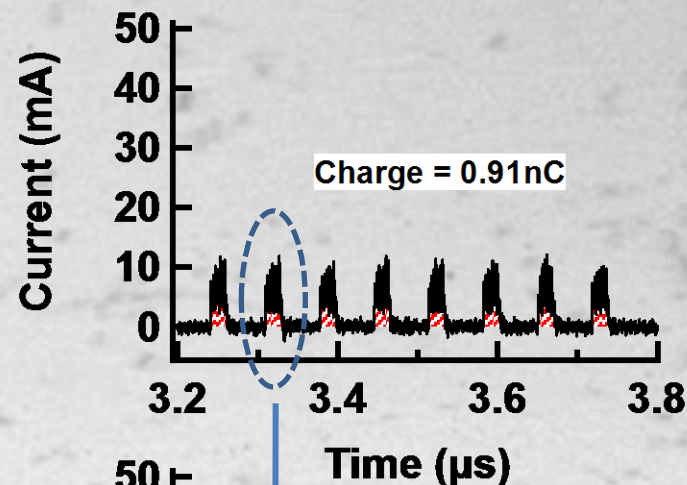
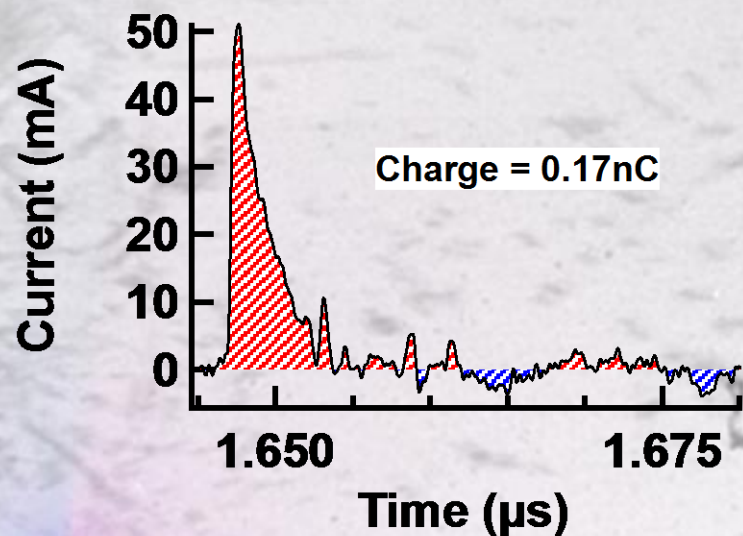
Long term stability



Pulse Mode Beam Position 11-ID-D, APS



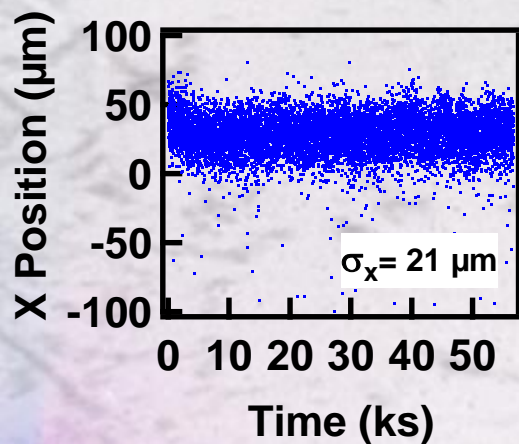
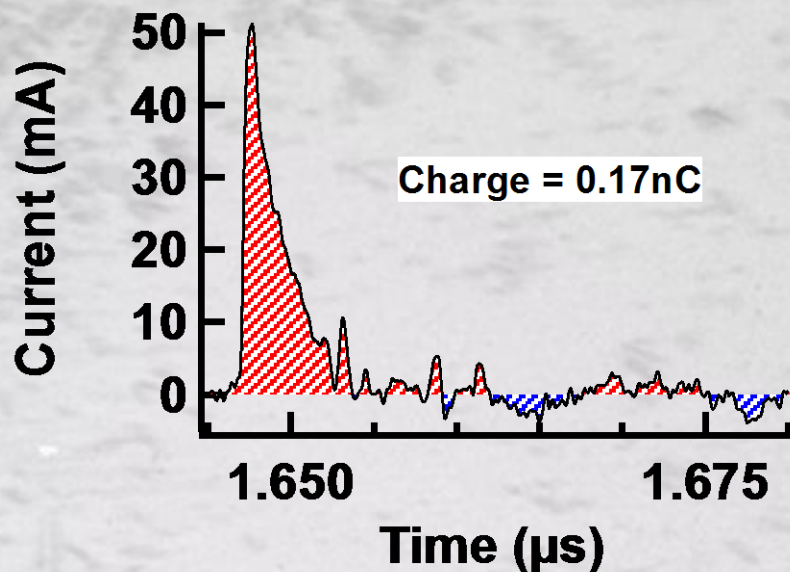
- Ring mode “hybrid fill, top up”.
- 102mA total, 16mA in first bunch, 86mA in remaining pulse train.
- Separated by 1.594 μs
- Ratio of ring currents matches very closely to measured charge ratio
- *Current Ratio: $86\text{mA}/16\text{mA} = 5.38$*
- *Measured Q Ratio: $0.91\text{nC}/0.17\text{nC} = 5.35$*



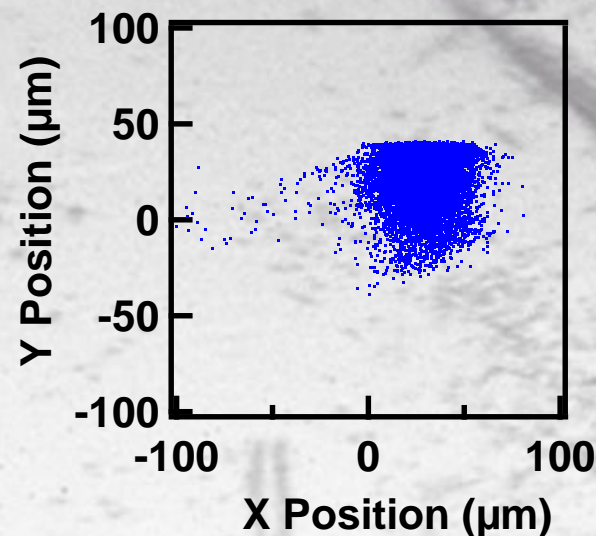
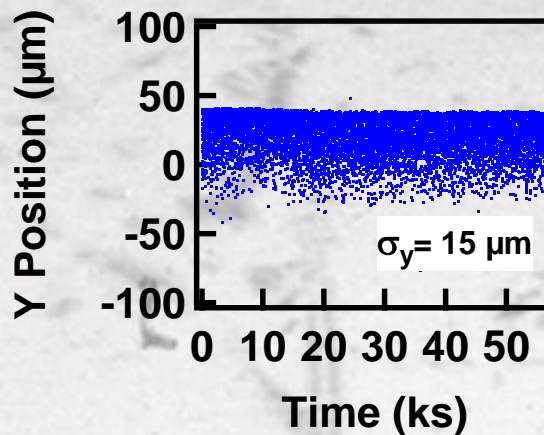
Pulse Mode Beam Position 11-ID-D, APS

Ring Structure at APS 11-ID-D

- Ring mode “hybrid fill, top up”.
- Tracked the singlet bunch position every 11 turns ($40\text{ }\mu\text{s}$) for 15 hrs
- Singlet bunch has a peak current density of 200 A/cm^2
- ***Traditional alignment feedback works on average current -> looking primarily at pulse train, not at singlet***



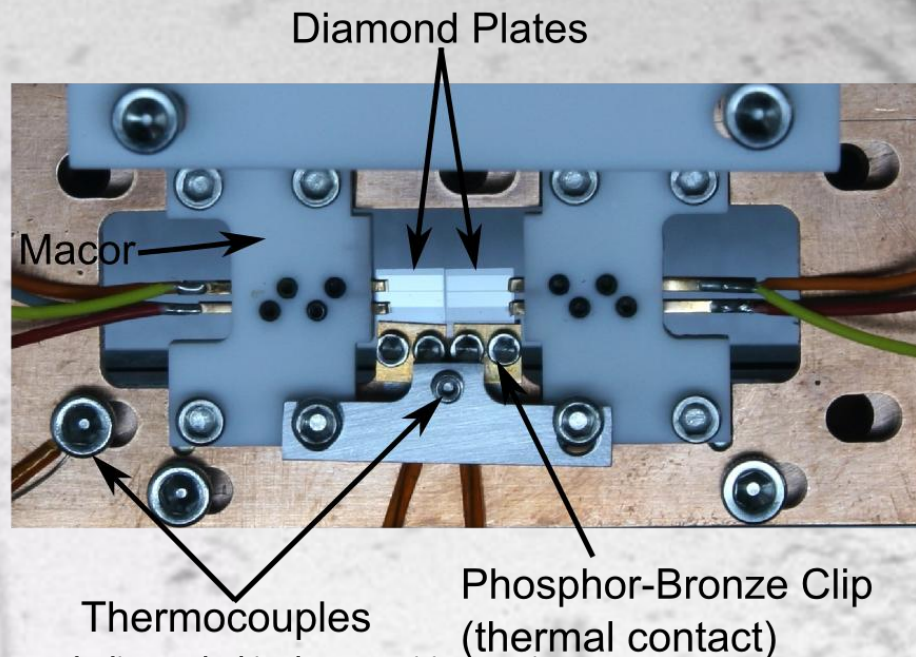
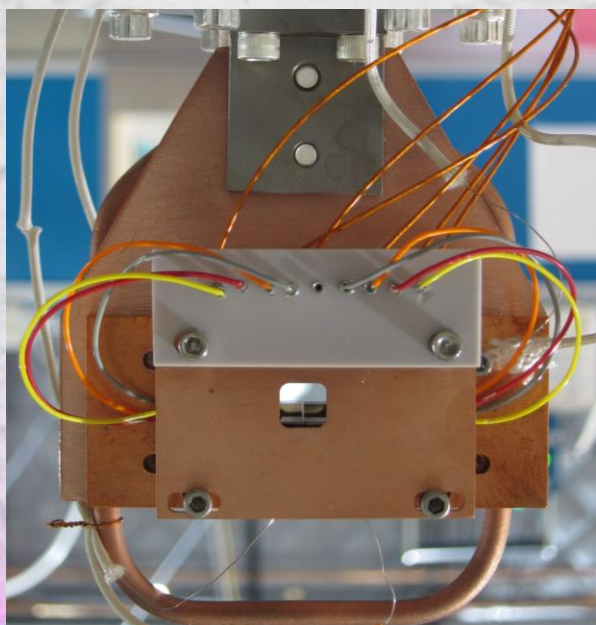
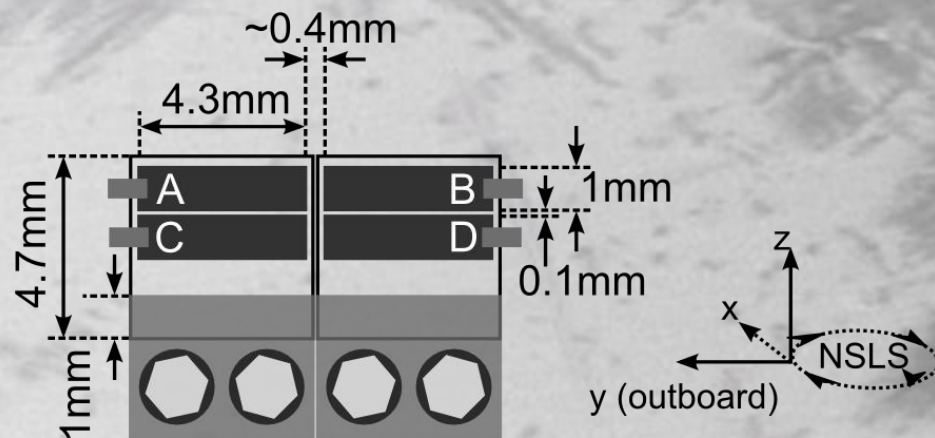
Long term stability



X25 White Beam Position Monitor

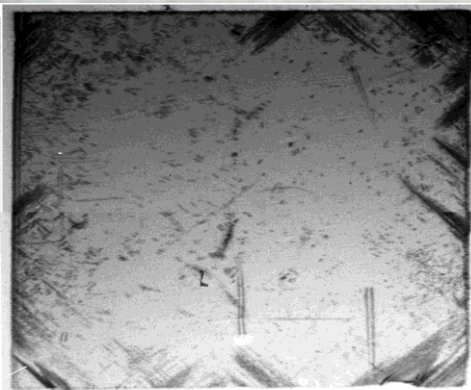
- Installed 13.6 m from undulator at X25
- Large ($6 \times 1 \text{ mm}^2$) beam; up to 100 W, 11W absorbed
- Two 100 μm thick E6/DDI single crystal diamond plates tiled side-by-side
- Selected with topography
- Custom 4-channel current amplifier
- Up to 760 mA observed
- Position noise:

Better than $0.5 \times 0.05 \text{ }\mu\text{m}$



Transmission-mode diamond white-beam position monitor at NSLS

E. M. Muller, J. Smedley, J. Bohon, X. Yang, M. Gaowei, J. Skinner, G. De Geronimo, M. Sullivan, M. Allaire, J. W. Keister, L. Berman and A. Héroux
J. Synchrotron Radiation, **19**, 381-387 (2012)



\overleftarrow{g}

$\overline{2}\overline{2}0$

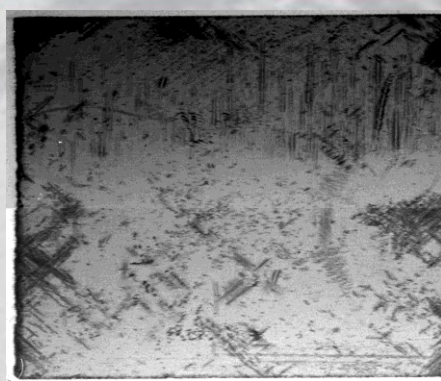
1441B



\overleftarrow{g}

$\overline{2}\overline{2}0$

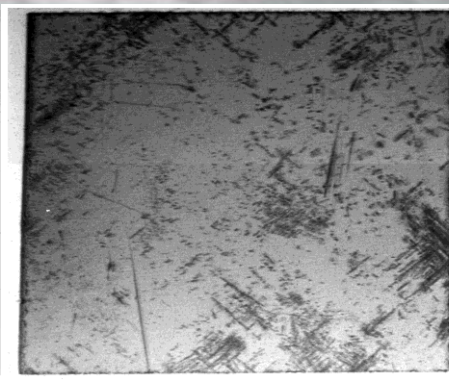
1443A



\overleftarrow{g}

$\overline{2}\overline{2}0$

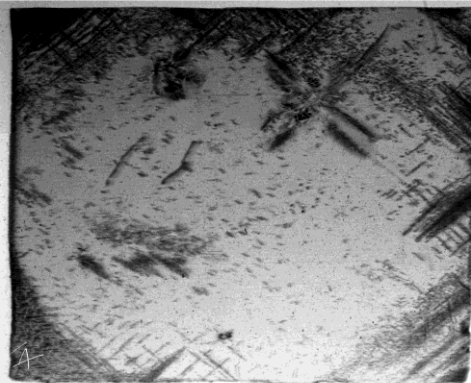
1443B



\overleftarrow{g}

$\overline{2}\overline{2}0$

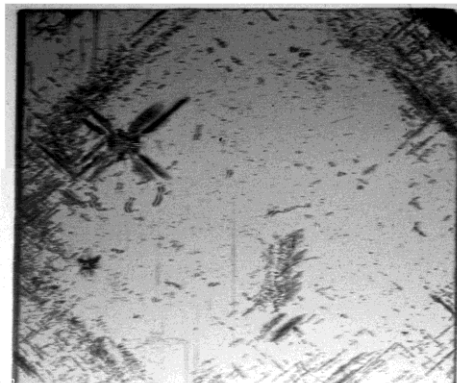
1447B



\overleftarrow{g}

$\overline{2}\overline{2}0$

1690A



\overleftarrow{g}

$\overline{2}\overline{2}0$

1690B



\overleftarrow{g}

$\overline{2}\overline{2}0$

1694A



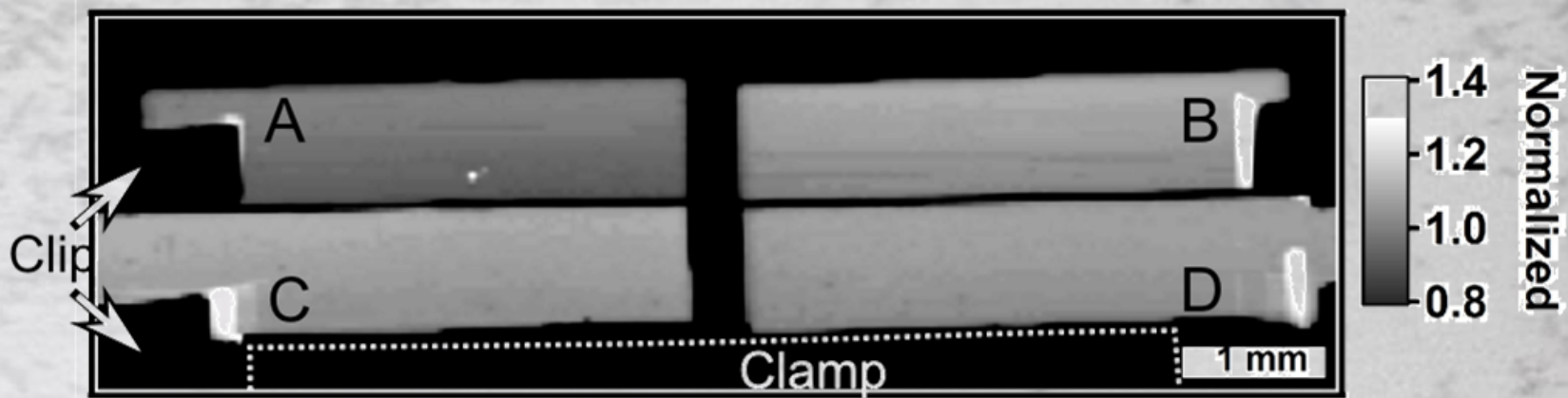
\overleftarrow{g}

$\overline{2}\overline{2}0$

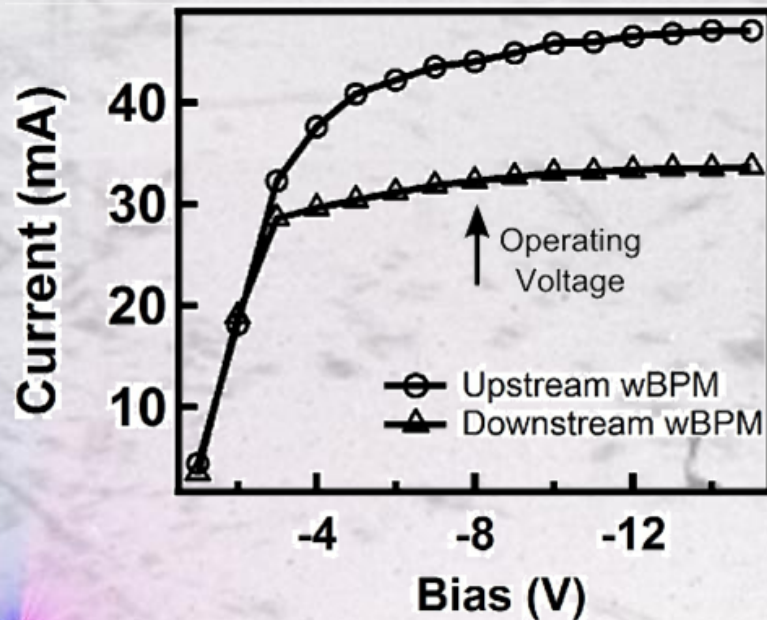
1694B

Monitor Calibration

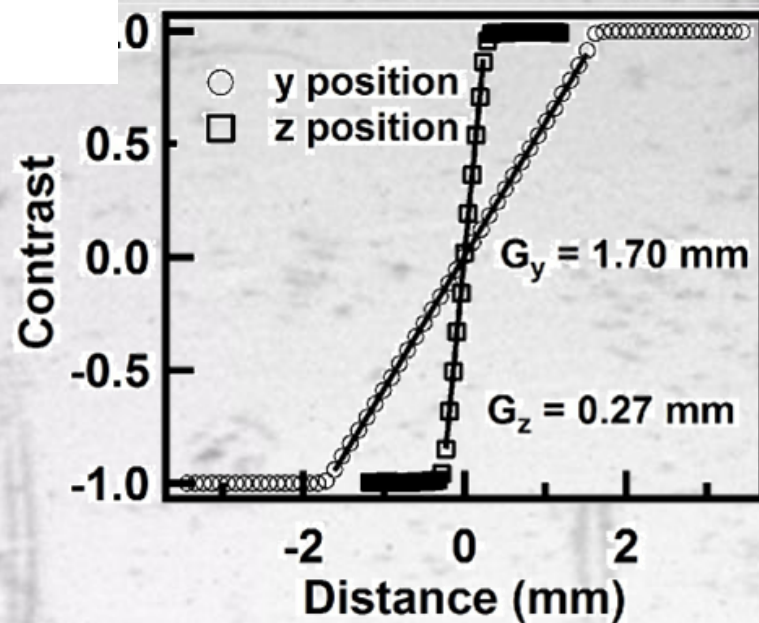
XBIC Map



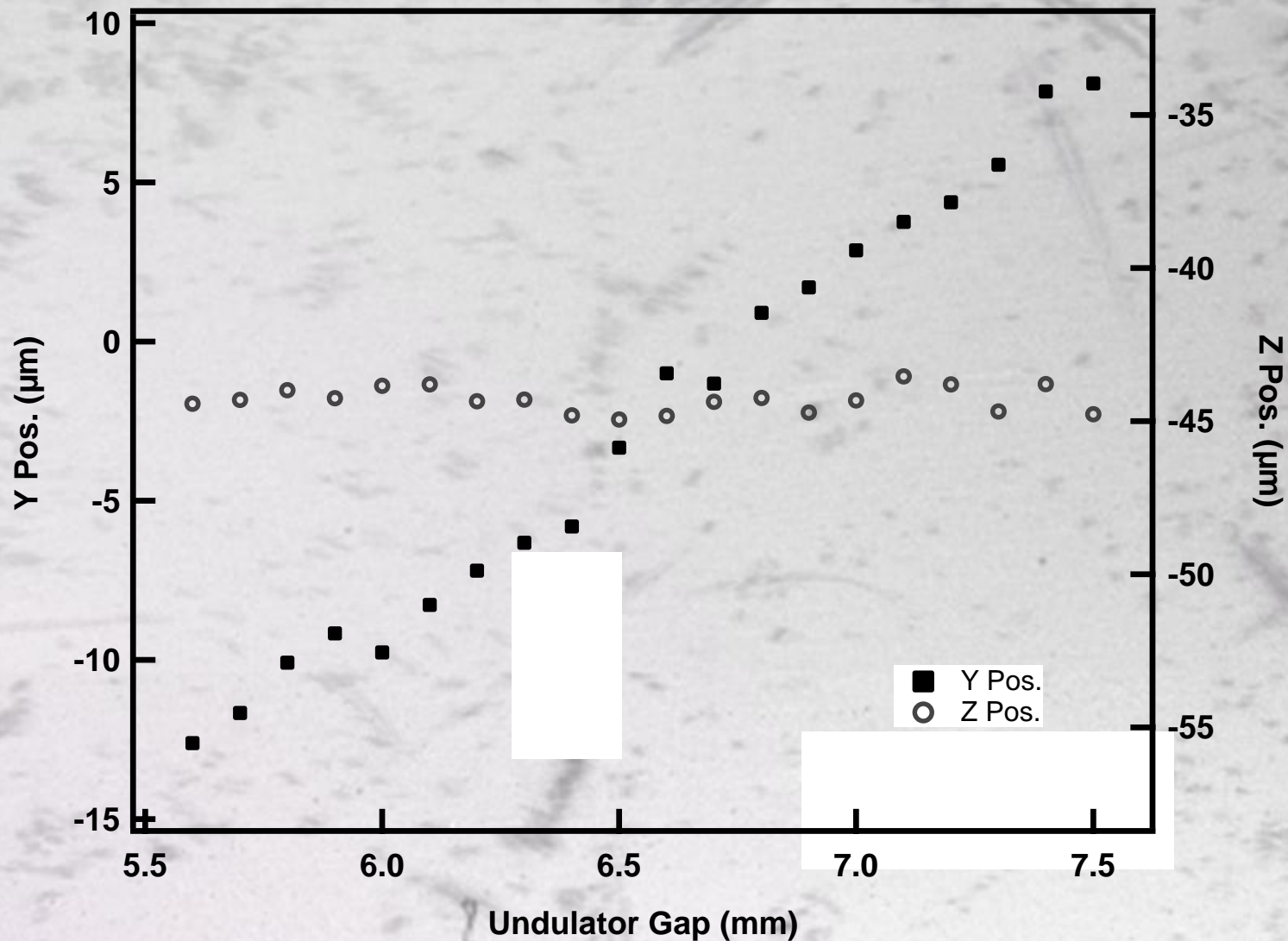
Bias Calibration



Position Calibration



Monitor Results

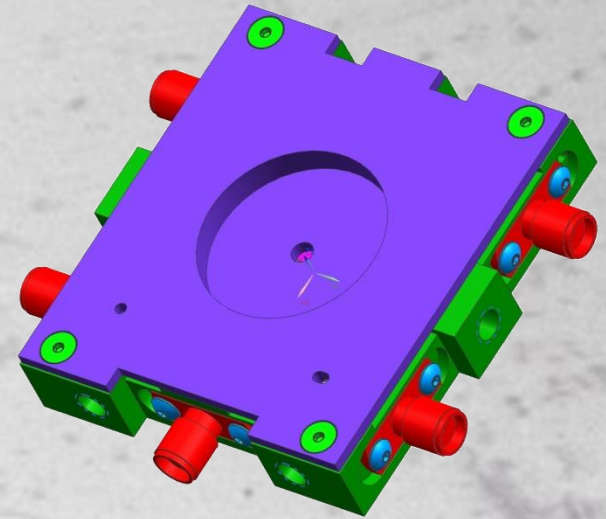


Moving electron beam changes photon beam position

Beam position changes with undulator gap

Extent of motion is a function of e-beam position

- *Sydor Instruments, LLC* is actively collaborating with BNL in developing the Diamond BPM technology.
- SBIR Phase II awarded for FY2013-2014.
Phase IIa just awarded for 2015-16
- Currently developing prototypes for white beam and monochromatic beam applications.
- User requirements is driving commercial development.



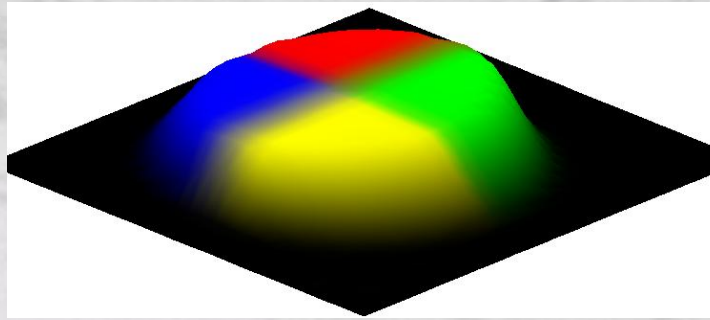
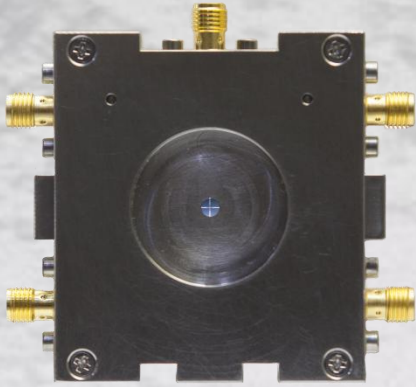
For more information please contact:

Jaime Farrington

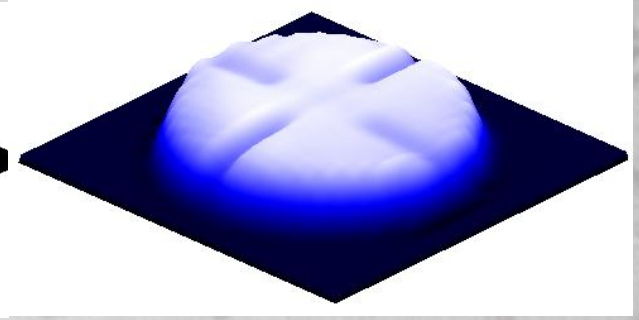
jaimef@sydorinstruments.com

585-764-9584

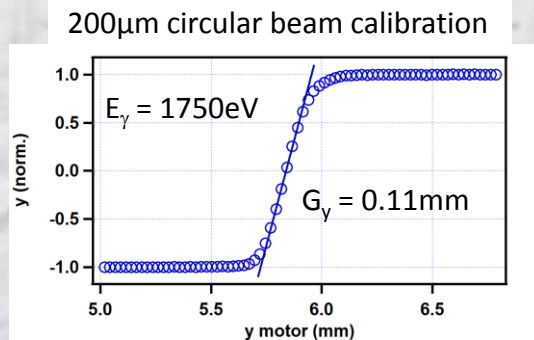
Sydor Quad Results



$E_\gamma = 4\text{keV}, -5\text{V DC}$



$E_\gamma = 3\text{keV}, 0.3\text{V } 90\%$



This is for -20V on incident, 90% duty cycle

For 1.6mm beam:

Gx=0.74mm

Gy=0.76mm

For 0.8mm beam

Gx=0.35mm

Gy=0.36mm

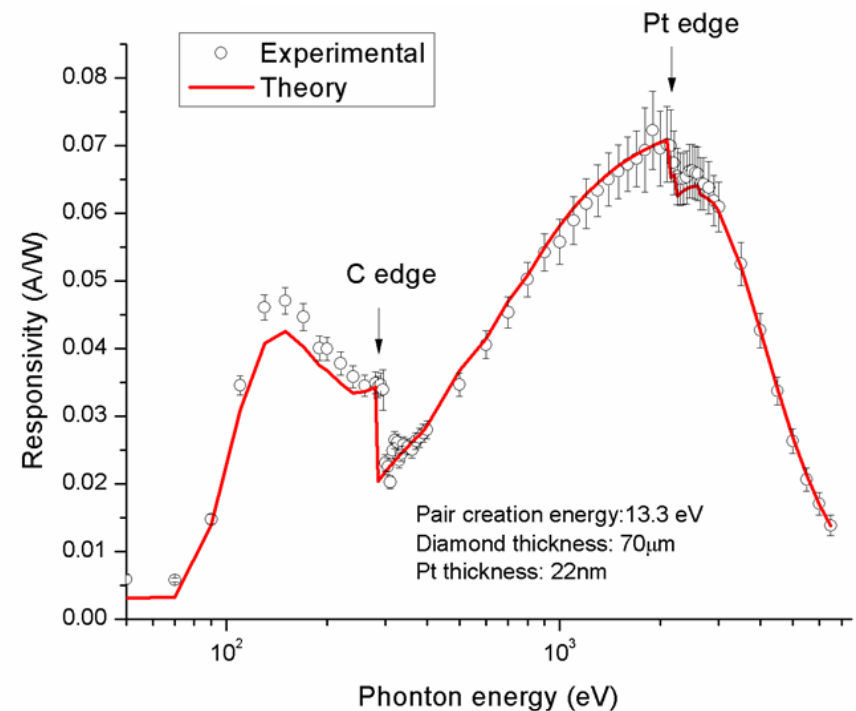
For 0.4mm beam

Gx=0.27mm

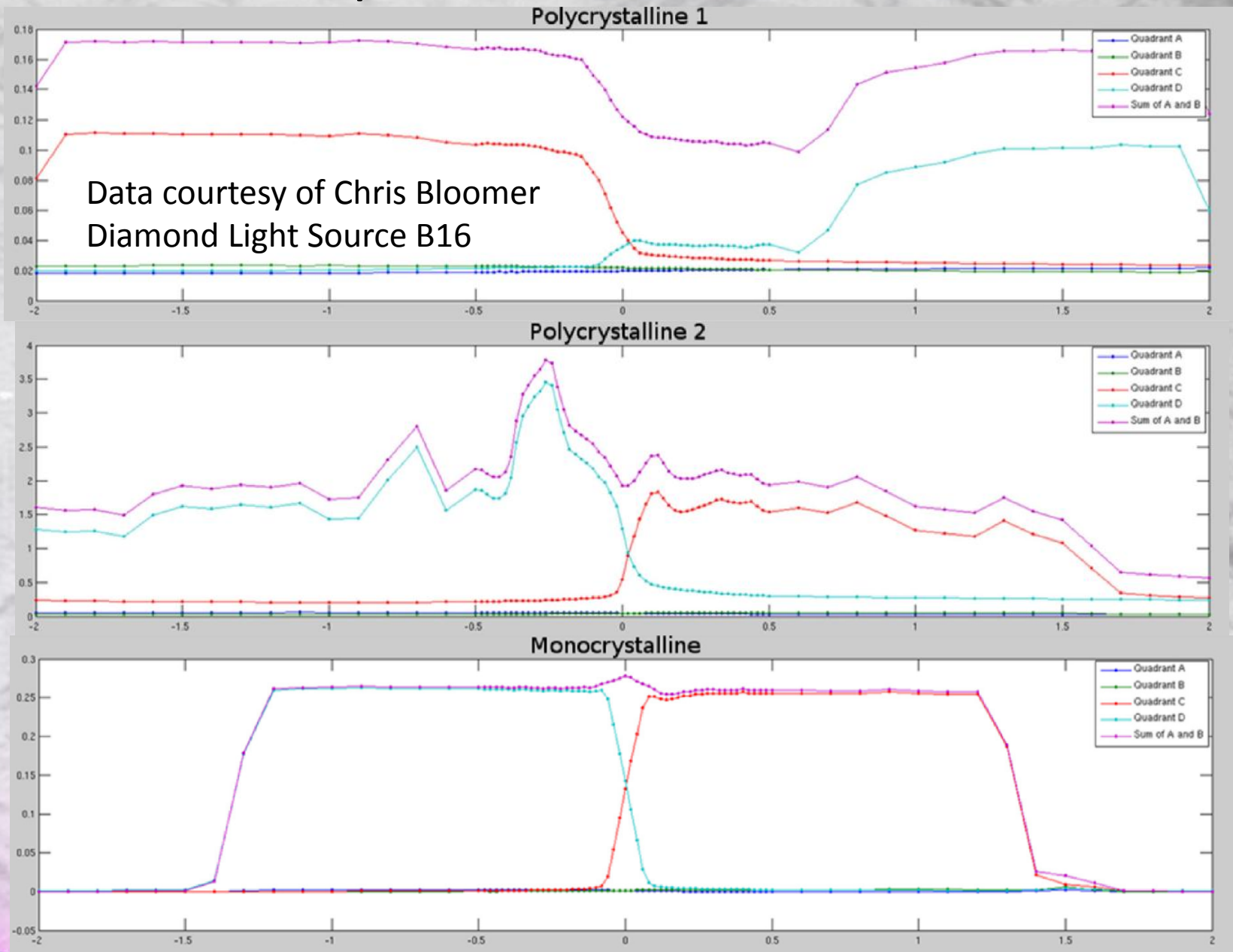
Gy=0.19mm

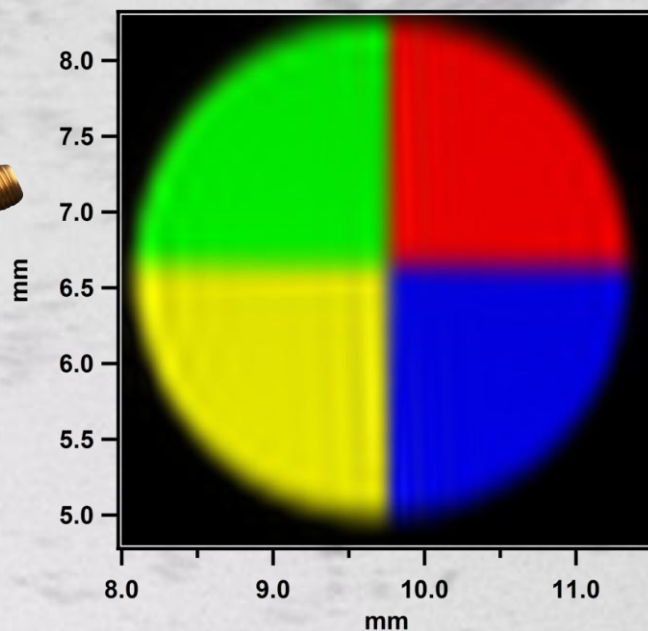
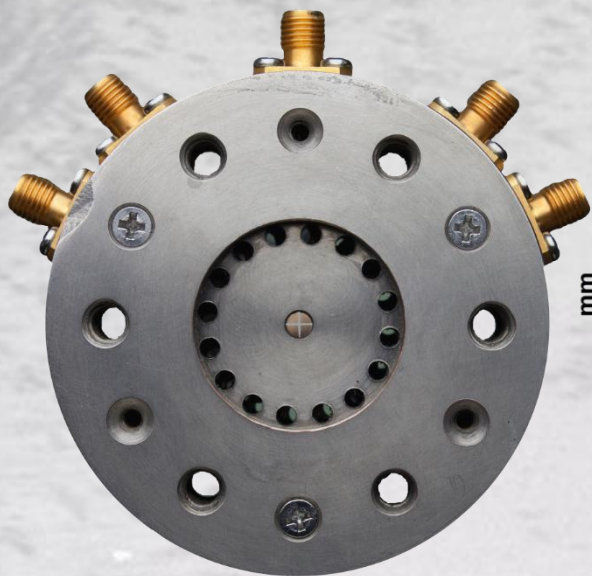
Photon energy for 68 μm attenuation length = 3850eV

Energy Calibration



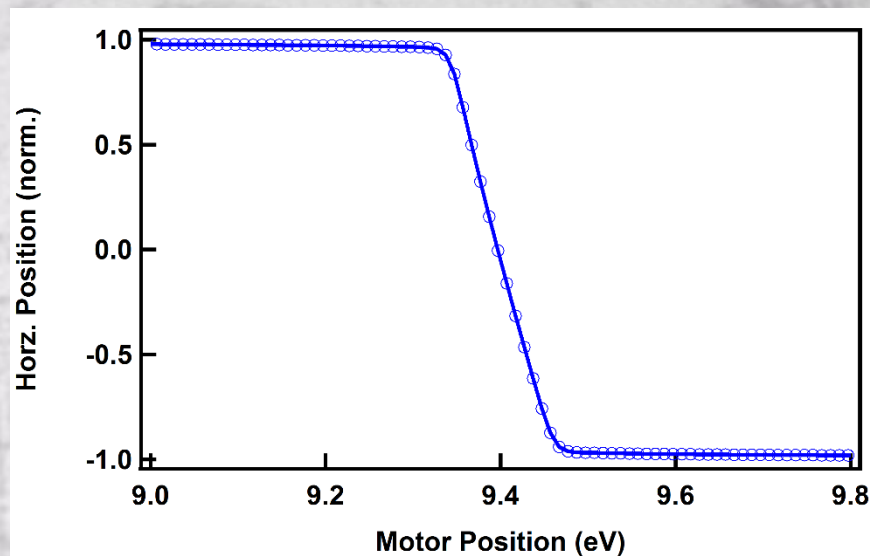
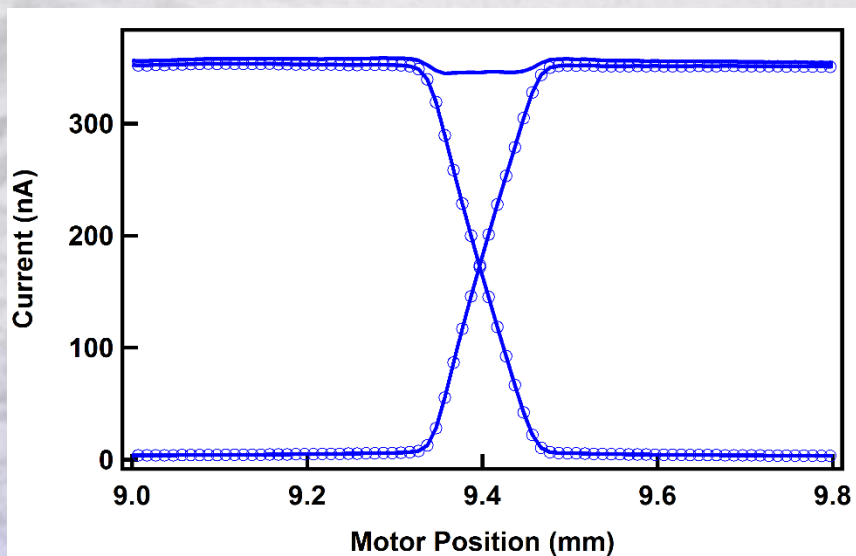
Comparison to Dectris DBPM





Quad detectors for NYSBC

- 2 quad detectors (65 μ m and 80 μ m thick)
- 3.6mm x 3.6mm x 30nm Pt contacts, 20 μ m streets
- High thermal conductivity ceramic circuit board (Beryllia)
- Integrated vacuum seal
- Operating voltage 10V.
- Self-aligning defractometer



Readout options

- Single channel devices can be read by current amplifiers and digitizers, as ion chambers
- Quadrant devices can be read out several ways
 - Adapting NSLS II eBPM readout
 - Two versions: RF and electrometer
 - RF version measures impulse response rather than current
 - May allow utilization of lower grade of diamond
 - Take advantage of existing NSLS II integration
 - Custom 4-channel current amplifier
 - 4-channel electrometer
 - Sydor marketing these



Diamond Instrumented Window

Development of a diamond window which will provide position, flux and morphology of high flux x-ray beams while simultaneously acting as the vacuum-air interface.

X-ray footprinting (XFP) at NSLS-II

- Focused white beam
- Variety of beam sizes/shapes needed
- Feedback and control systems for optical elements or sample positioning stages.

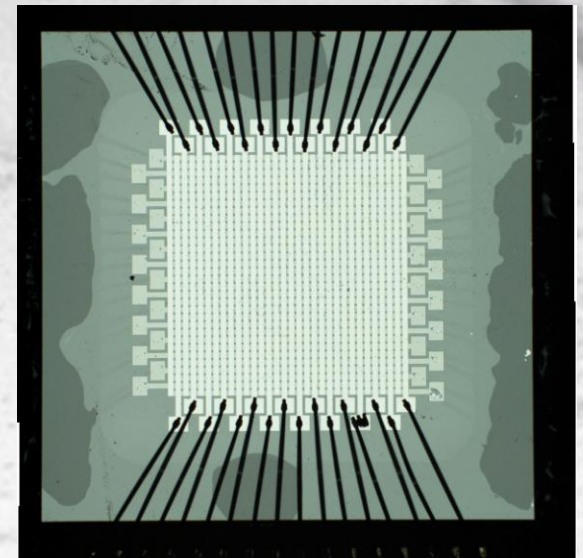
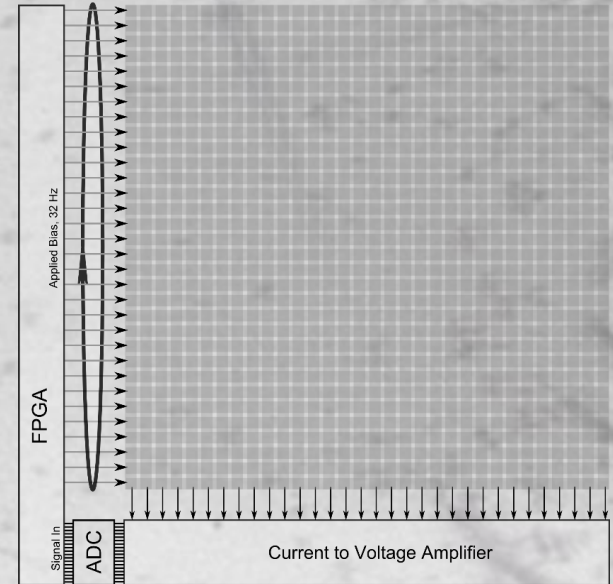


Image Readout

- Goal of 32 x 32 stripes, yielding 1024 pixels
- Only one row is active at a time minimizing ohmic heat generation.
- Real-time imaging at 32 Hz
- Allows for feedback control of beamline components.

Major Challenges for high flux beamlines

- Heat load management in optics (including beryllium windows)
- Real-time volumetric measurement of beam properties such as flux, position, and morphology.



Current and Future Work

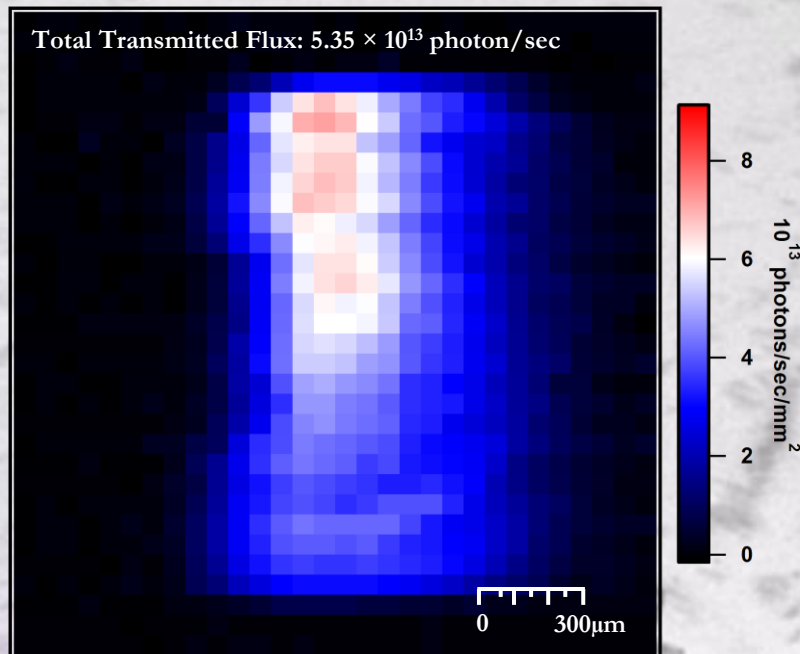
Instrumented window

- Design, fabricate and test assembled vacuum window
- Increase the dynamic range to extend to lower flux measurement

SAXS detector

XAS flow cell

Diamond Imaging Detector @ CHESS, G3



- G-line: Three station beamline with common 49-pole wiggler source
- Can deliver high flux monochromatic beam
- Horizontal and vertical focusing

What do we want out of an electron source?

- The electron beam properties determine the photon beam properties
 - Pulse duration, degree of coherence, flux
- In all light sources through 3rd generation, the phase space is determined by the ring

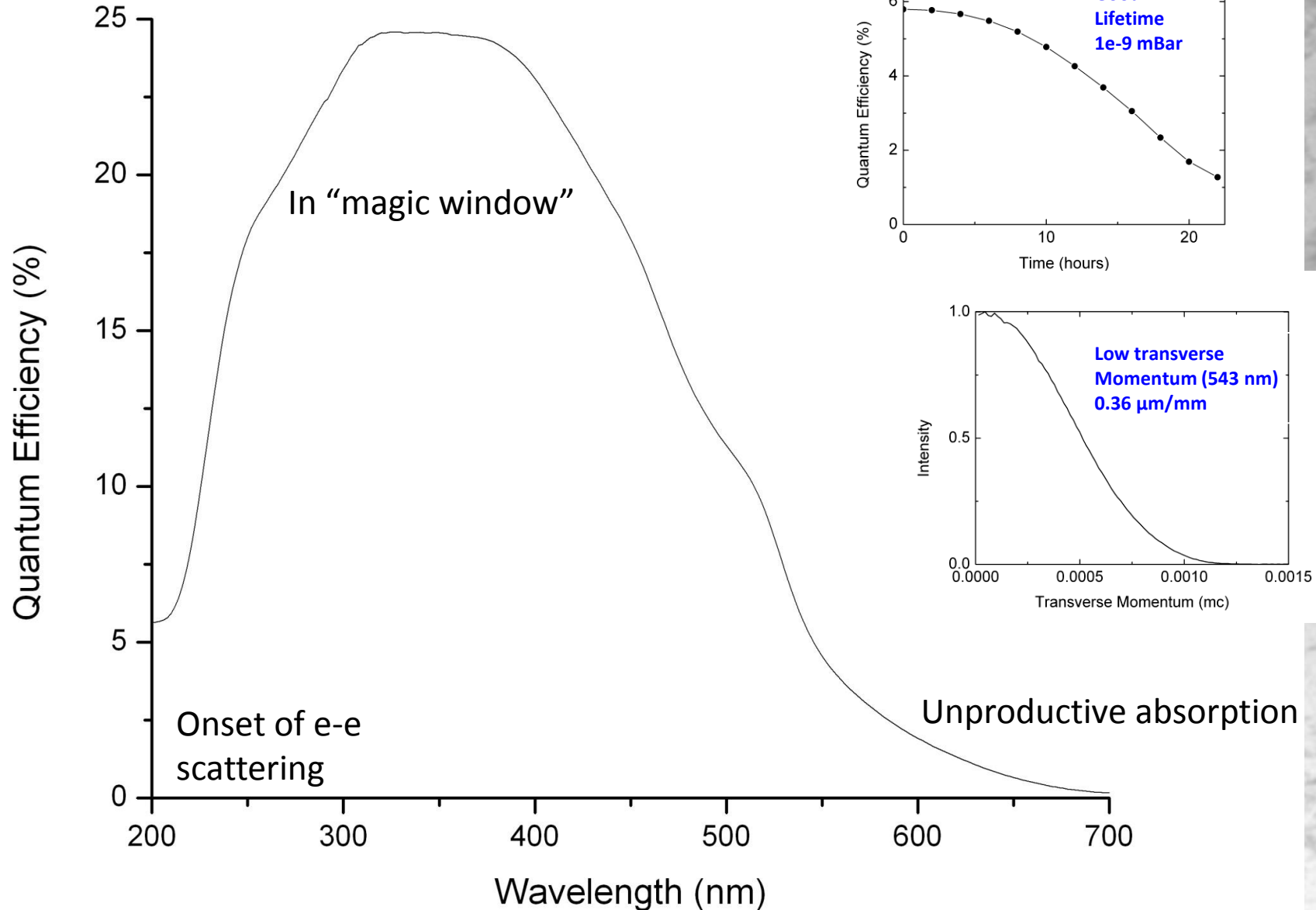


- In 4th generation sources (LCLS, XFEL, NGLS), this will change
 - the electron source will determine the beam properties
- The highest brightness sources available are photoinjectors, which use a laser on a photocathode to control the spatial and temporal profile of the emitted electron beam

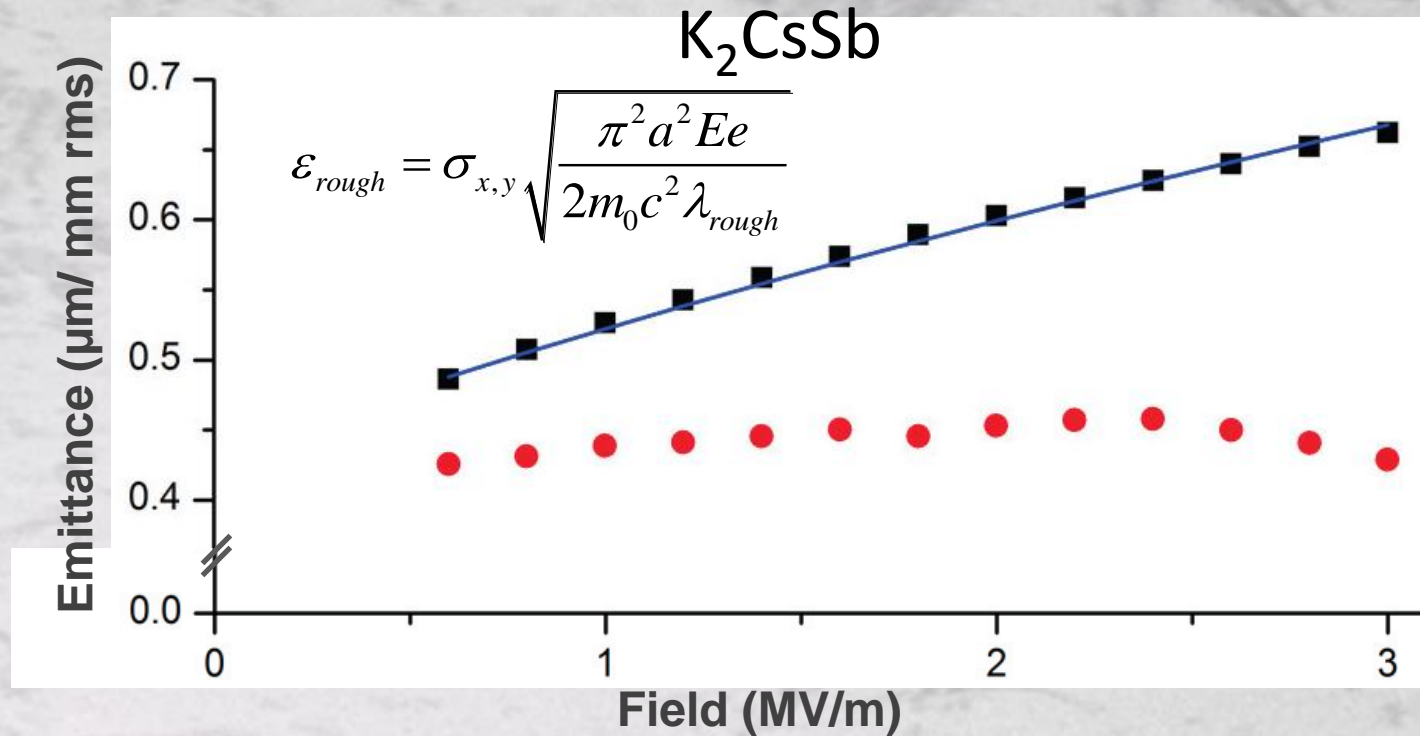
What do we want out of photocathode?

- High Brightness: $B = \frac{N_e}{\varepsilon_{nx}\varepsilon_{ny}\varepsilon_{nz}}$
 - large number of electrons in a small volume of phase space
 - Low Emittance: $\varepsilon_n = \sigma_x \sqrt{\frac{\hbar\omega - \phi_{eff}}{3mc^2}}$
 - Determines the electron energy required for an X-FEL at a given wavelength $\varepsilon \approx \frac{\lambda}{4\pi} \Rightarrow \frac{\varepsilon_n}{\beta\gamma} \approx \frac{\lambda}{4\pi}$
 - High Quantum Efficiency
 - High Average Current
 - Long Operational Lifetime
 - Chemical Contamination
 - Ion back bombardment
 - Sub-ps response time
- The optimal cathode is still a work in progress*
- It is becoming increasingly clear that material parameters such as texture and surface roughness may play an important role*

K_2CsSb : A cathode with excellent characteristics for accelerators



Effects of roughness seen in the emittance of thick multilayer

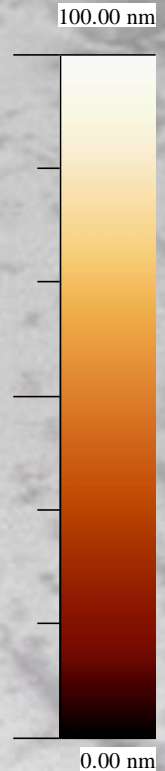
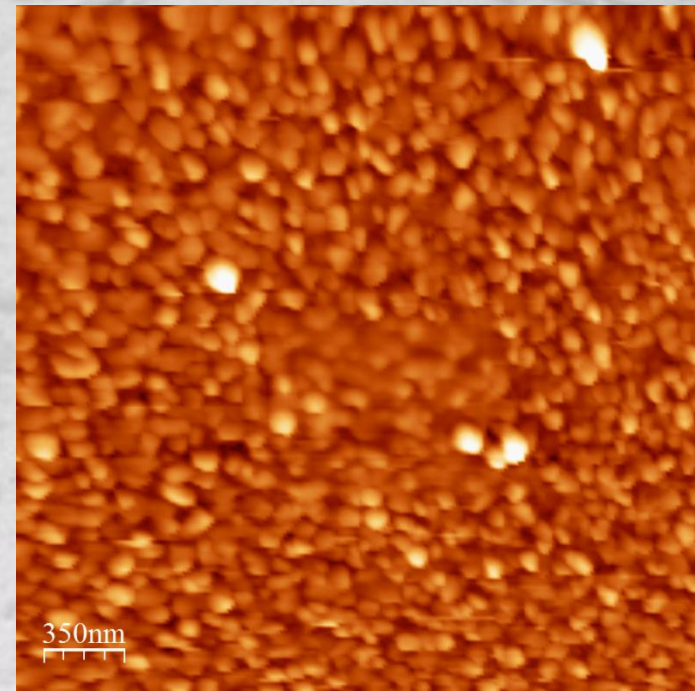
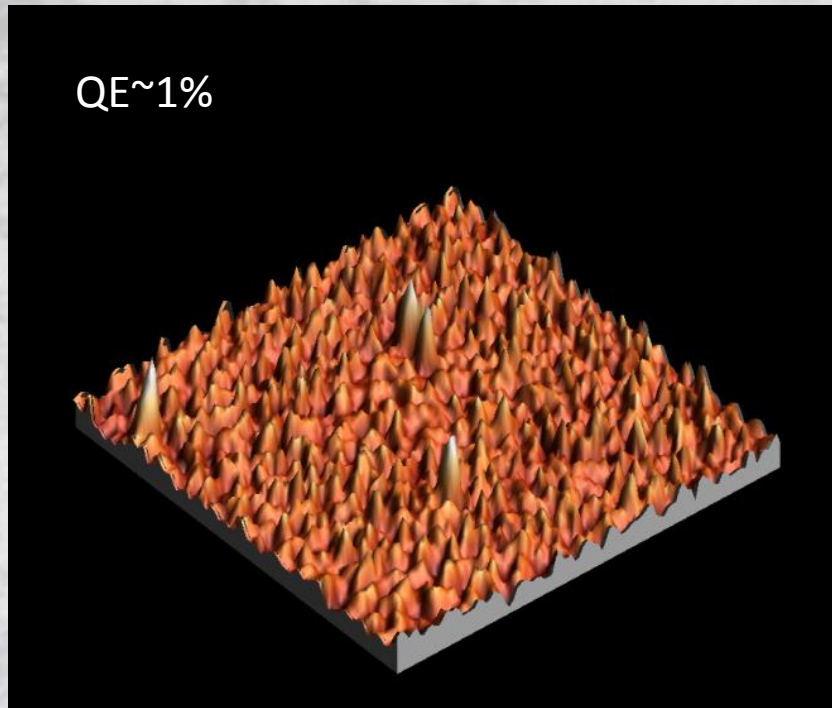


Thin films grown at high rate give \sim expected emittance (very low field dependence)
Films grown in a multilayered manner were shown to give higher QE but showed marked emittance growth with field
Can be explained by invoking a simple roughness model.

Fitting gave reasonable roughness parameters, confirmed by in vacuum AFM

Roughness in high gradient guns looks to be an issue based on current in-situ measurements of cathode surfaces

in-situ AFM on cathode at CFN



10 nm Antimony film evaporated at room temperature

Potassium and Cs added by monitoring QE

Should result in a 50 nm thick final film

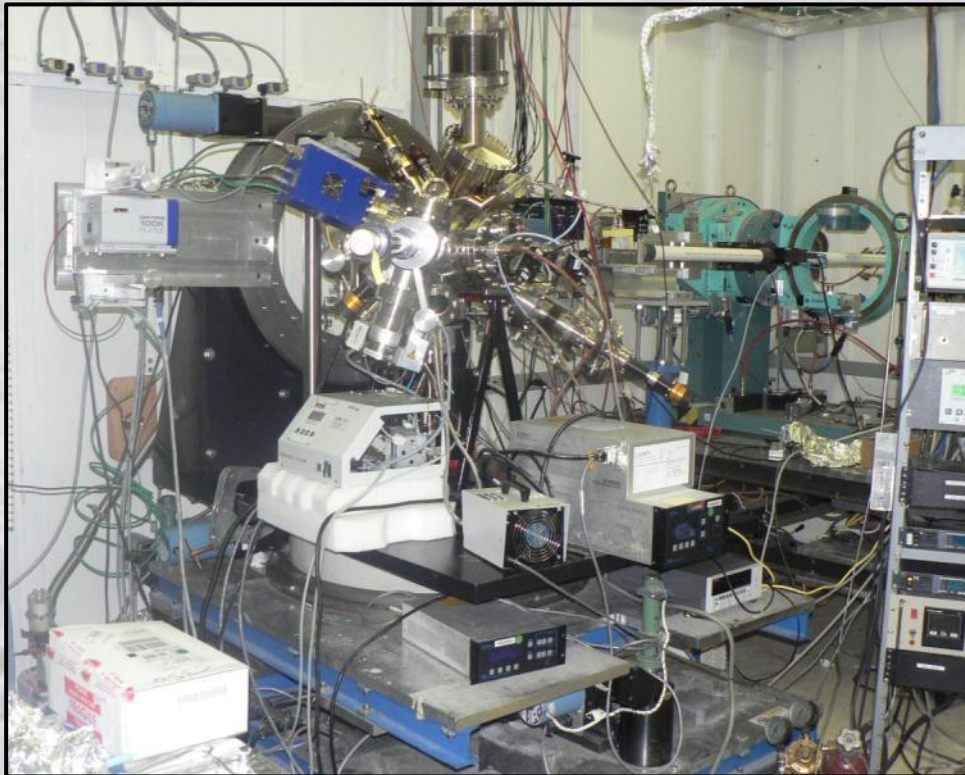
Observed **25 nm** RMS roughness, with a 100 nm spatial period

Nano-pillars of uniform height – consistent with XRR and GISAXS

Likely the source of the Field dependence of the intrinsic emittance

S. G. Schubert, et al, APL Mater. **1**, 032119 (2013)

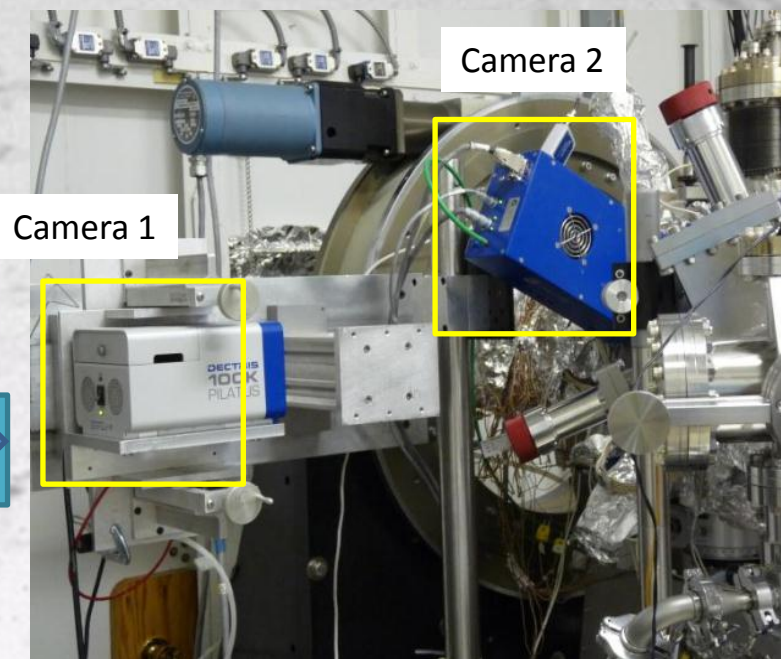
In operando analysis during growth (setup at NSLS/X21 & CHESS G3)



- UHV system (0.2 nTorr base pressure)
- Residual Gas Analyzer (RGA)
- Heating/cooling substrate/cathode
- Load lock
 - fast exchange of substrates
 - gun transfer
- Horizontal deposition of Sb, K and Cs.

Two 2D detectors (Pilatus 100K) →

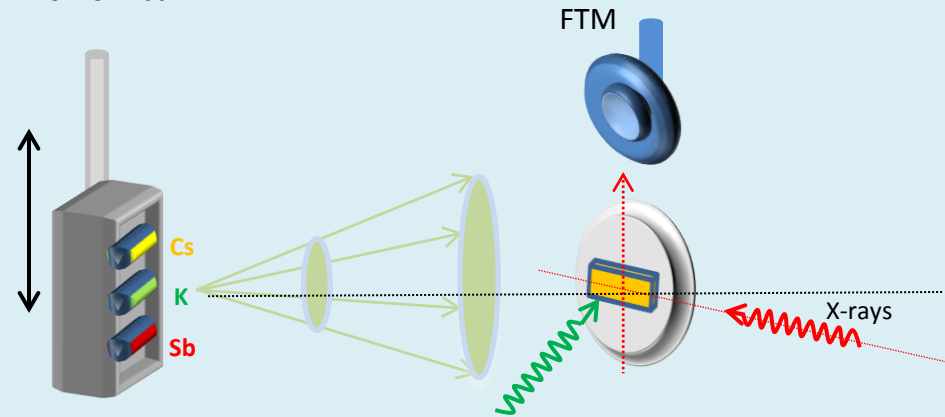
Next Stop: ISR at NSLS-II



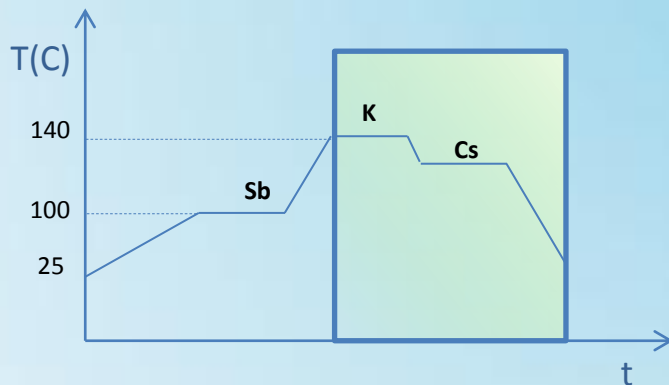
Experimental set up: K_2CsSb cathode growth

Horizontal evaporation of three sources:

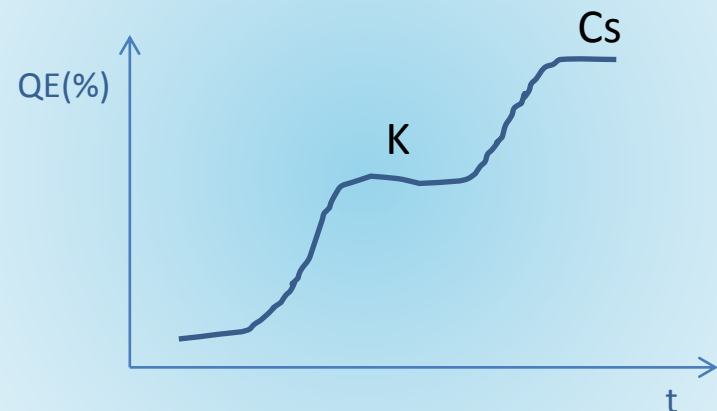
$P=1 \times 10^{-10}$ mbar



Recipe:



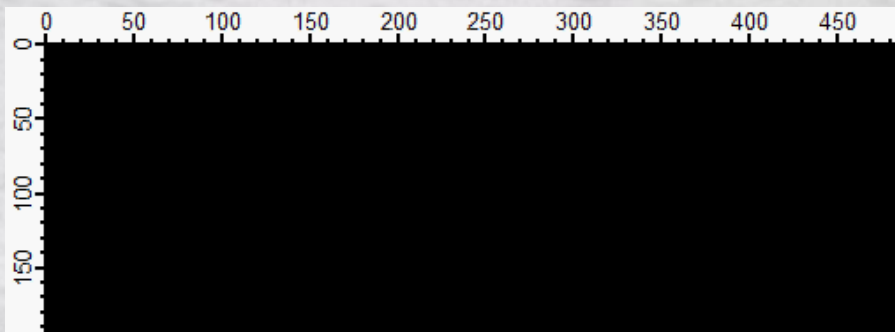
QE during growth (532 nm laser)



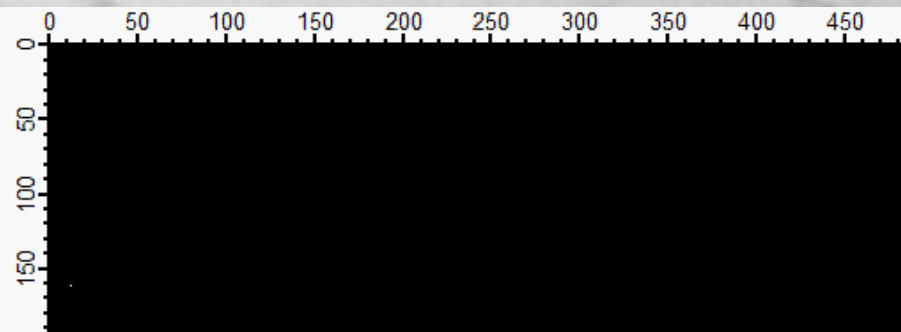
Simultaneously Acquire XRD and GISAXS

- Understanding reaction dynamics through crystalline phase evolution
- Map the thickness and roughness evolution of the cathode
- Is there a correlation between reactivity, QE and roughness?

Camera 1: GISAXS & XRR



Camera 2: WAXS



time

0 Å

165 Å

14.9° 39.3°

(003)

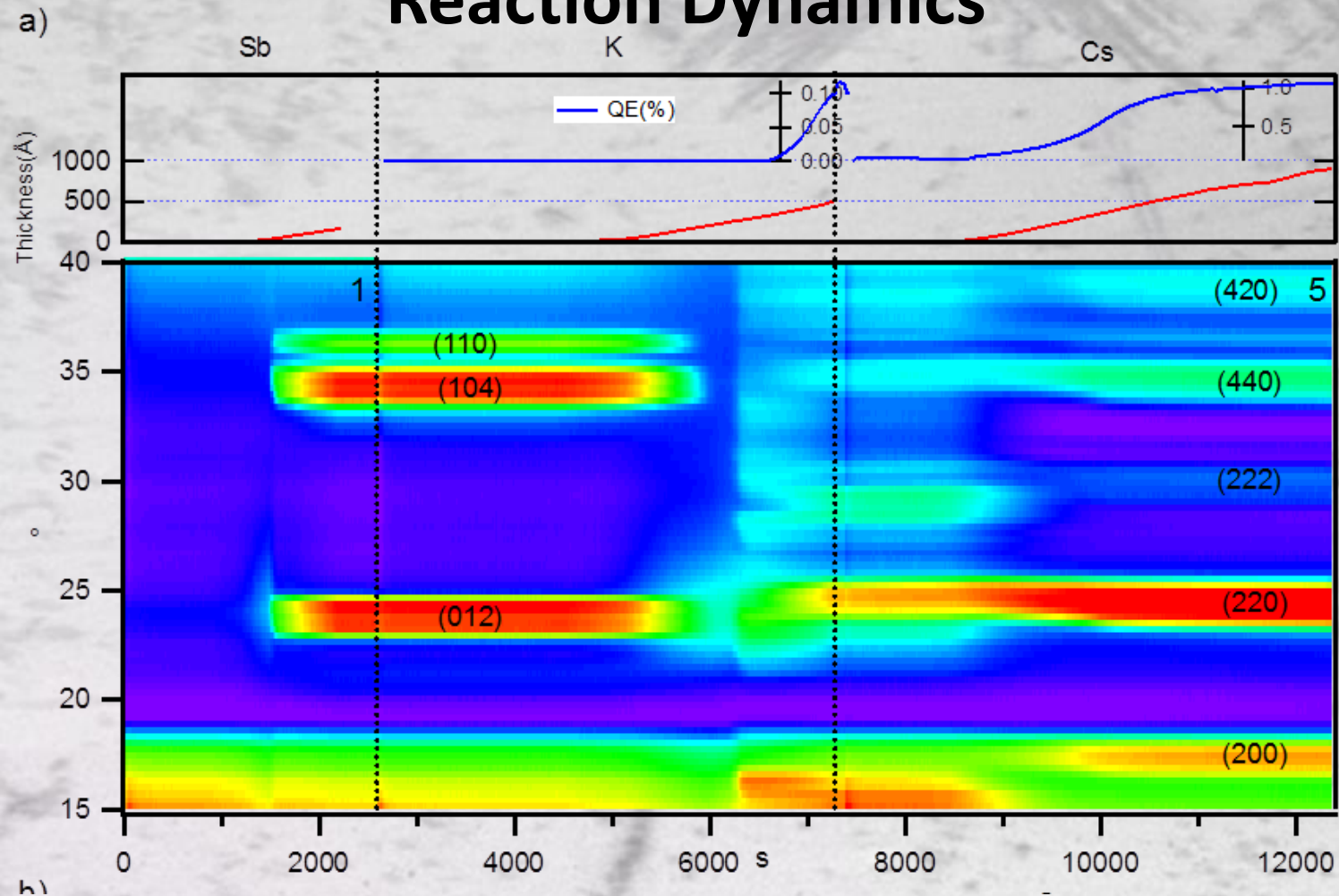
(012)

(104)

(110)

Sb peaks

Reaction Dynamics



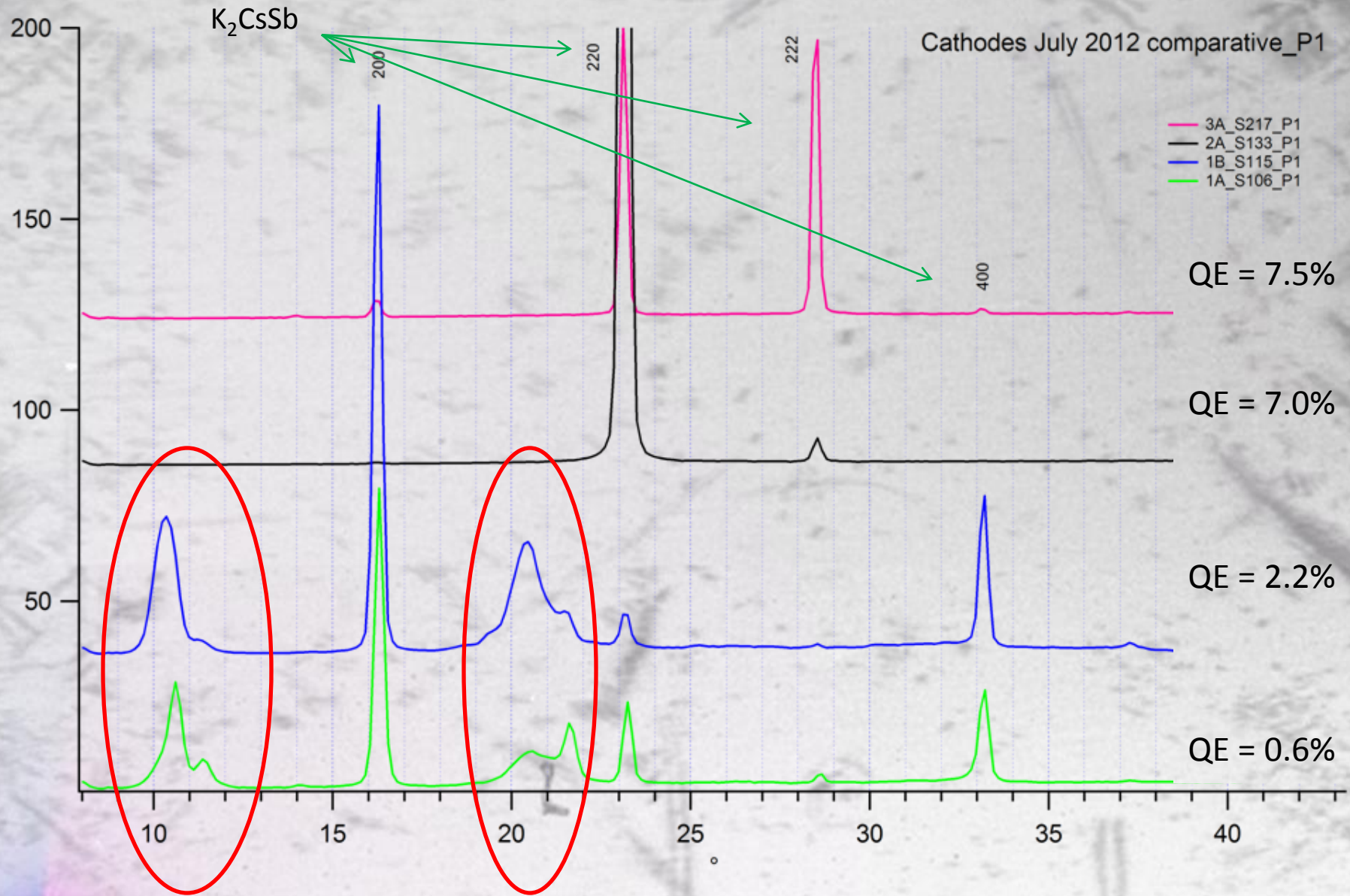
Antimony evaporated on Si, 0.2 Å/s ; crystallize at 4nm
K deposition dissolves Sb layer - This is where roughening occurs!

QE increase corresponds with $K_x\text{Sb}$ crystallization

Cs increases lattice constant and reduces defects

M. Ruiz-Osés et al., APL Mat. 2, 121101 (2014)

Comparison of Crystal structure and Final QE



Engineering a Smoother Cathode

Idea: Never let Sb crystalize

First layer:

3 nm Sb @ 100C

12 nm K @ 125C QE 0.16 %

42 nm Cs @ 125C QE 3.1 %

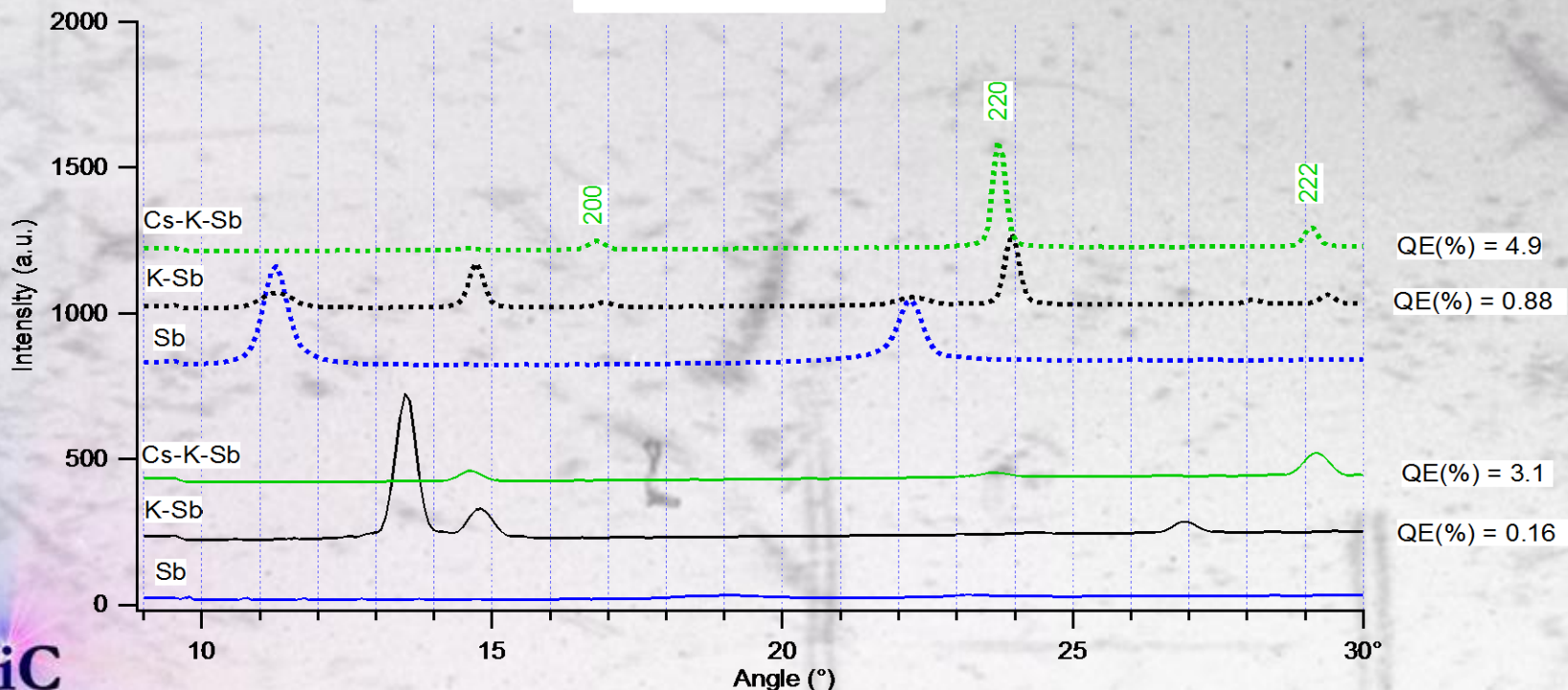
Second layer on top of first

Second layer:

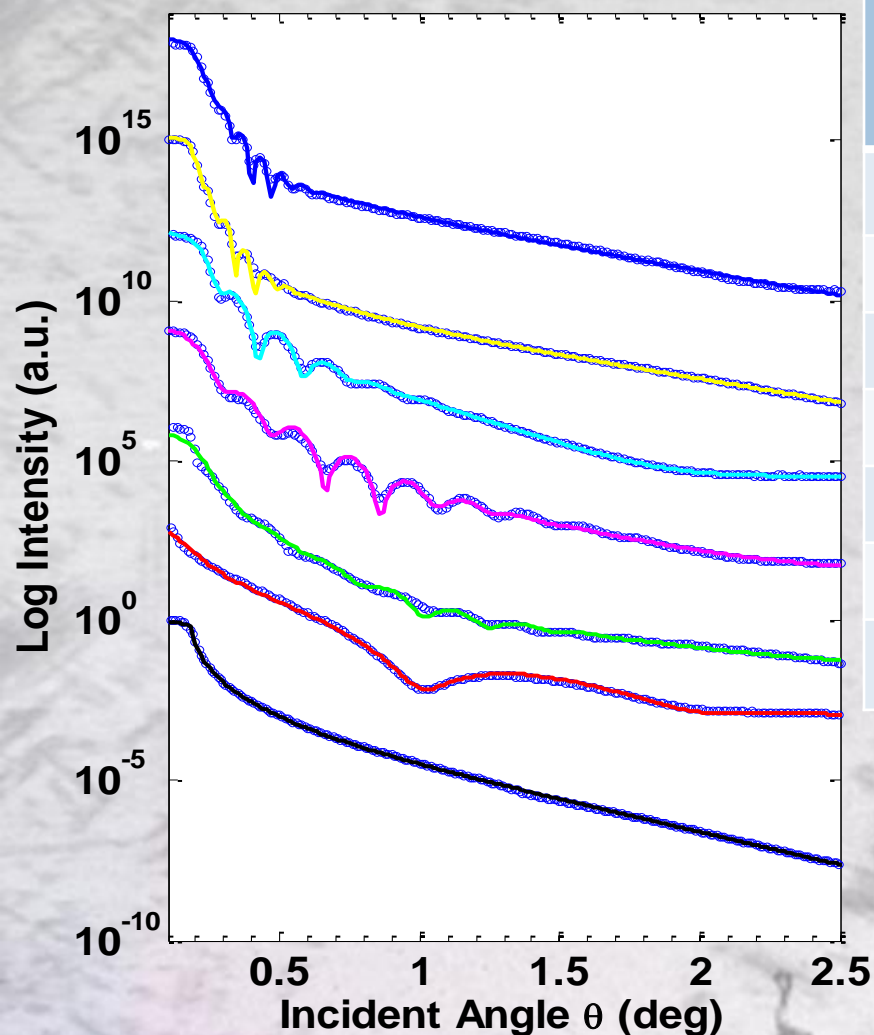
5 nm Sb @ 125C

16 nm K @ 125C QE 0.88 %

44 nm Cs @ 125C QE 4.9 %



XRR shows roughness evolution



Deposited Layers	Total Thickness (Å)	Roughness (Å)
Cs-K-Sb-Cs-K-Sb/Si	469	32
K-Sb-Cs-K-Sb/Si	449	36
Sb-Cs-K-Sb/Si	200	21.3
Cs-K-Sb/Si	174	13.2
K-Sb/Si	141	10.5
Sb/Si	35	2.9
Si Substrate	-	3.1

The substrate fit includes 1.5 nm of SiO_2

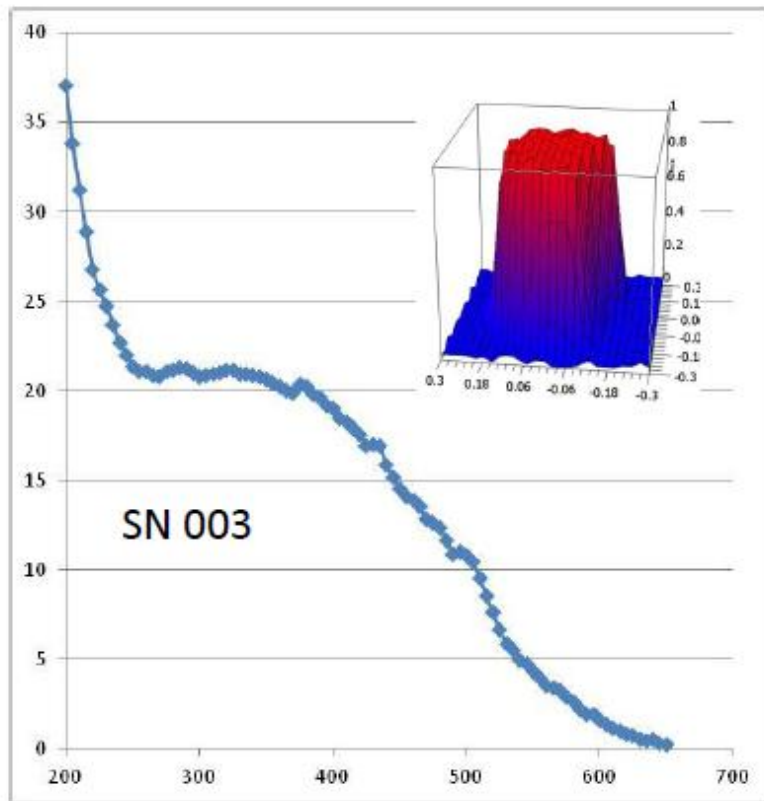
Multi-layer subcrystalline film is smoother,
At slight loss of QE

Next Stop: Sputter Deposited Cathodes

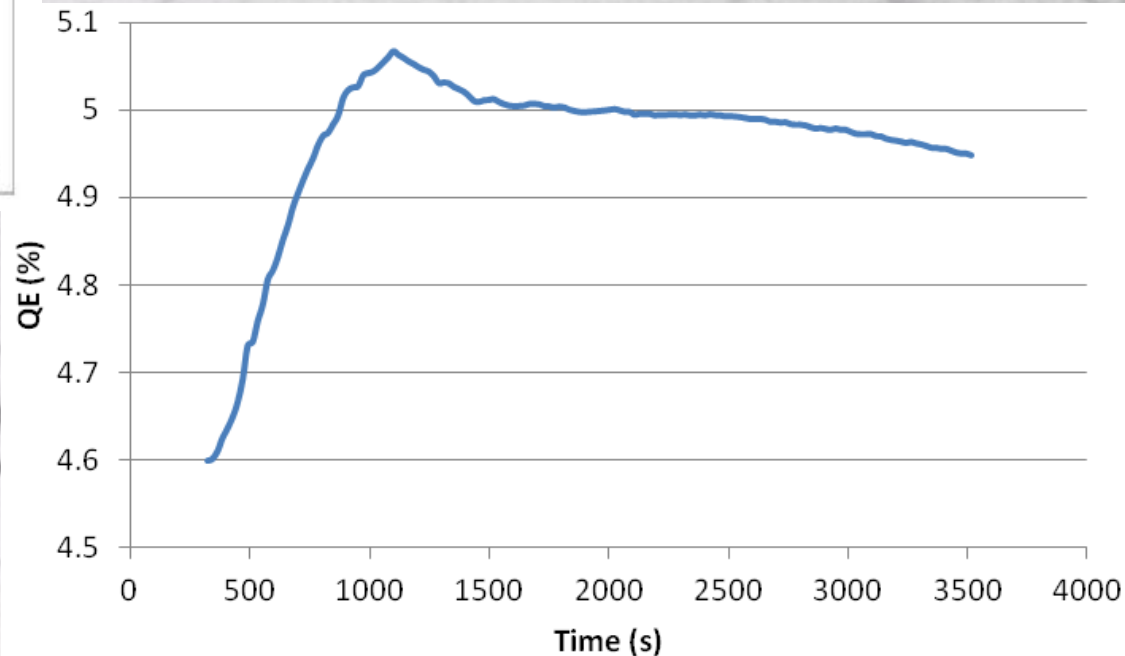
Sealed Capsule Photocathodes

Photonis USA, using detector
growth process

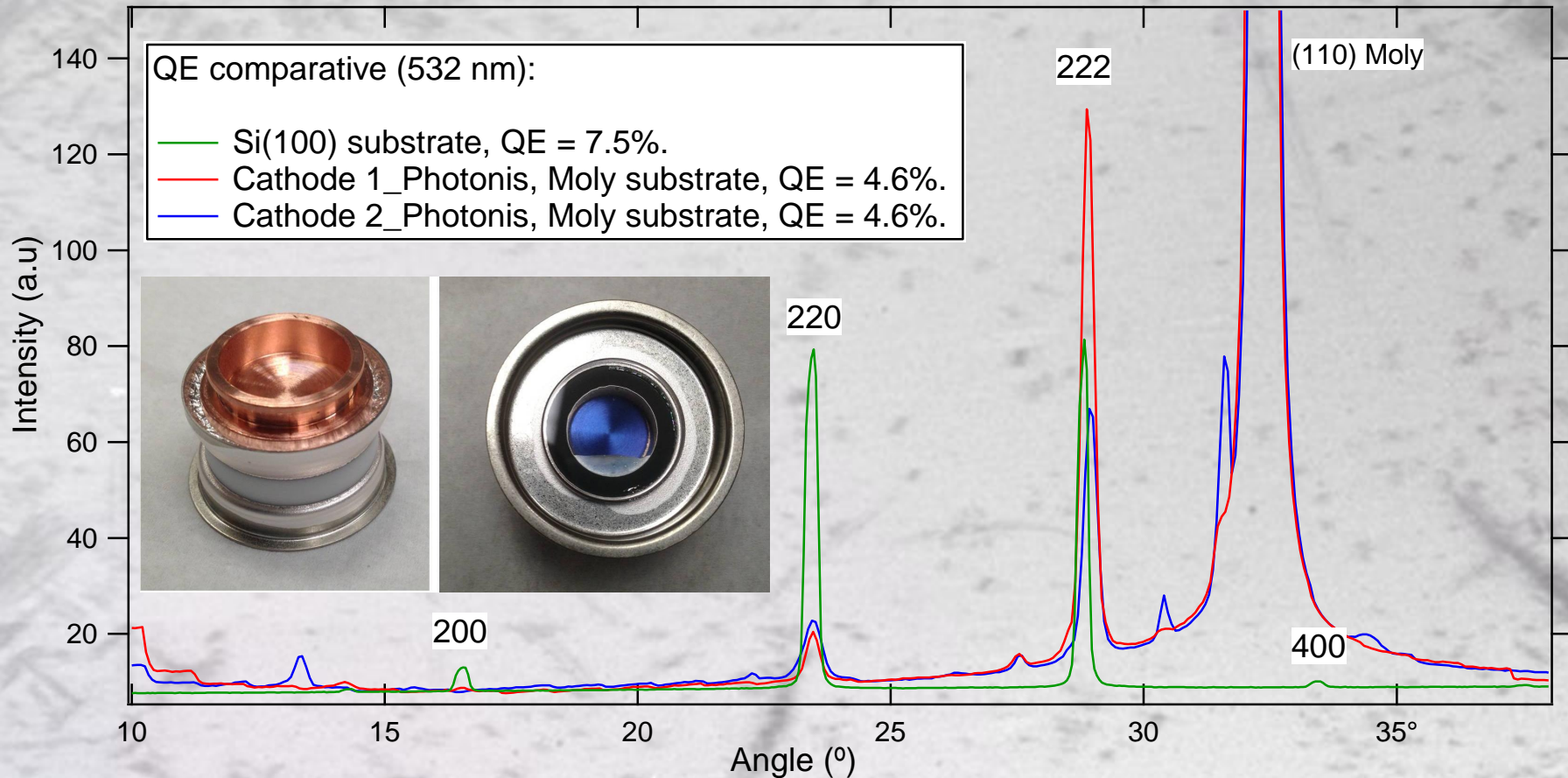
Shelf life of months at least
 NaK_2Sb available



QE drops during
heating to remove cap,
but recovers



Sealed Capsule Photocathodes



Comparison to Photonis commercial PMT cathode

Similar texture (222 surface normal preferred)

Broader peaks imply smaller grain size

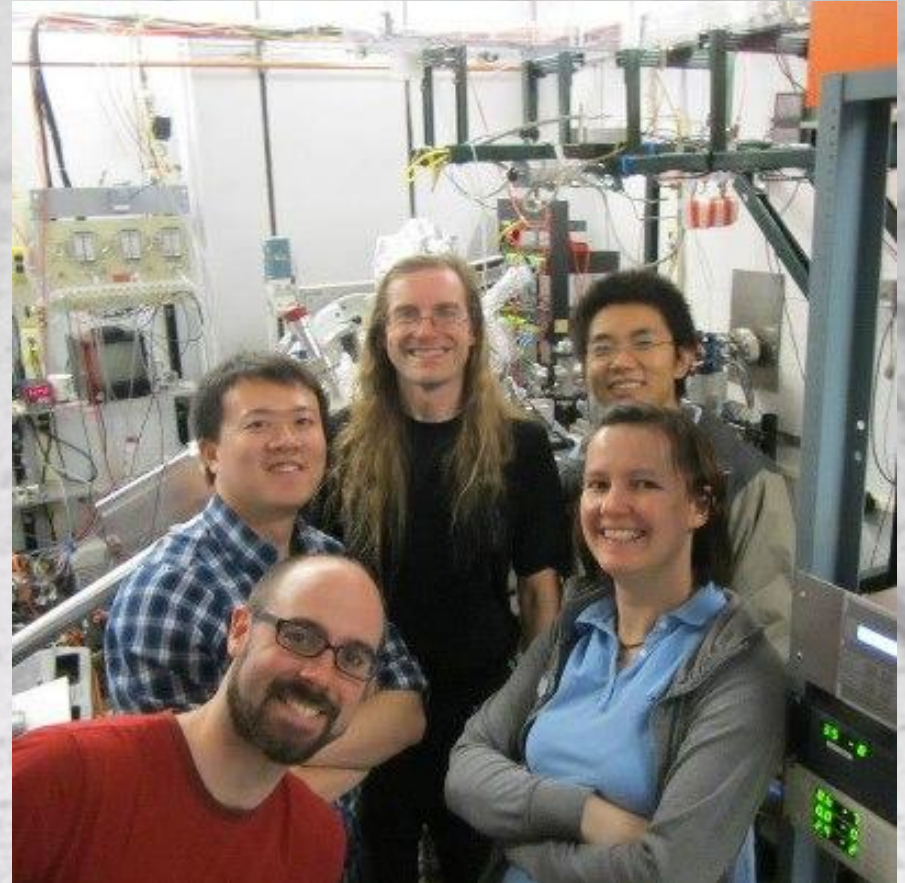
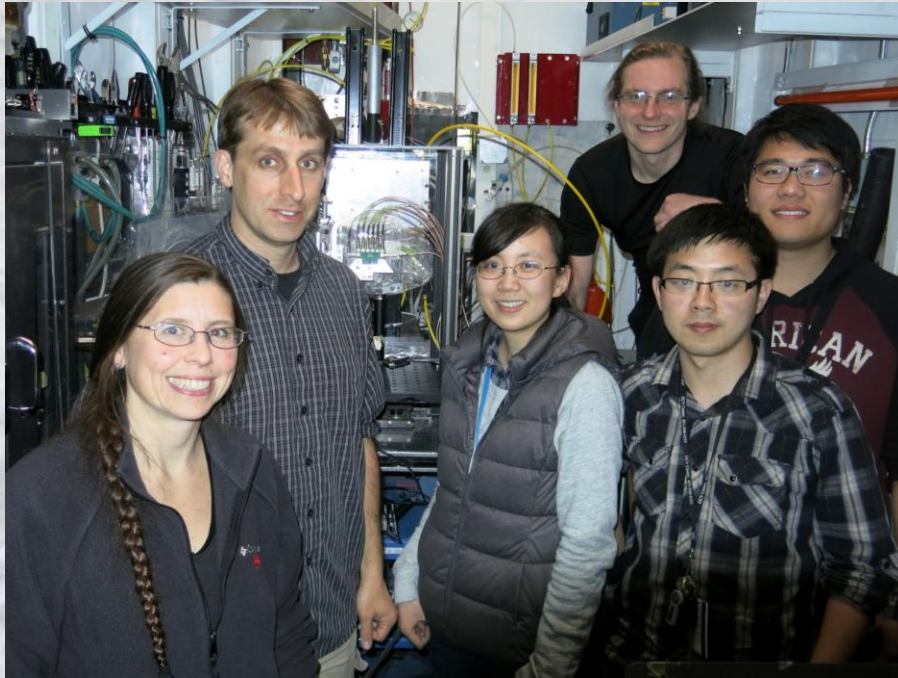
(50 nm for BNL cathode, 39 nm for Photonis cathode)

Conclusions

- From Photocathodes to X-ray diagnostics, we can use our tools to build better ones
- Alkali Antimonide cathodes
 - Peak QE of 35% and a green QE of 7.5% have been achieved
 - We are achieving control of both substrate and cathode crystal structure
 - Traditional cathodes are *very* rough... but we are learning to make them smoother
 - Sealed capsule cathodes may reduce cost and complexity in new user facilities
- Diamond
 - Flux linearity demonstrated over **11 orders of magnitude**
 - Persistent current/photoconductive gain results from point defects in the material, which can be screened for via topography
 - White beam beam position monitors have been in operation for 2 years
 - Position resolution of better than 50nm, and single bunch flux and position have been achieved
 - 50 devices delivered or on order world wide (APS, CHESS, Diamond, NSLS-II)
 - Polycapillary lenses solve the diffraction dropout problem for energy scanning applications, and allow high resolution EXAFS mapping
 - 1k Pixel beam imaging system demonstrated for both white and monochromatic beams

Thank you!

ELECTRON PHOTON INSTRUMENTATION CENTER



Thanks for your attention!

- Thanks to K. Attenkofer, J. Mead, W. Ding, T. Zhou, M. Maggipinto, A. Della Penna, T. Rao, S. Schubert, M. Ruiz Osés, J. Xie, J. Wang, H. Padmore, E. M. Muller, J. Bohon, J. Mead, M. Gaowei, A. Hérroux, L. Berman, M. Sullivan, R. Beuttenmuller, J. Jordan-Sweet, J. Keister, A. Sumant, E. DiMasi, J. Walsh, B. Raghothamachar, **J. Distel**, K. Vetter, G. DeGeronimo, B. Dong, D. Dimitrov, D. Pinelli, J. Skinner, M. Cowan, S. Ross, R. Tappero, B. Ravel, C. Jaye, D. Fischer, M. Lu, F. Camino, D. Abel, I. Ben-Zvi, T. Vecchione, X. Liang, J. Rameau, P. Johnson
- Beamlines (and staff): U2A, U2B, U3C, U7A, U13, X3B, X6B, X8A, X15A, X16C, X19C, X20A&C, X21, X23, X24, X25, X28C & APS ID 11D & CHESS G3
- DOE Office of Science – Basic Energy Science and High-Energy Physics, NSF IDBR Program

